Aus dem Institut für Herz- und Kreislaufphysiologie
(Prof. Dr. med. D.M. Katschinski)
im Zentrum Physiologie und Pathophysiologie
der Medizinischen Fakultät der Universität Göttingen

Characterization of the cytosolic and mitochondrial glutathione redox potential using cardiomyocyte specific transgenic Grx1-roGFP2 sensor mice

INAUGURAL-DISSERTATION

zur Erlangung des Doktorgrades
der Medizinischen Fakultät der
Georg-August-Universität zu Göttingen

vorgelegt von

Andrea Fecke (geb. Kesemeyer)

aus

Hildesheim

Göttingen 2023

Dekan:	Prof. Dr. med. W. Brück
Referentin:	Prof. Dr. med. D. M. Katschinski
Ko-Referentin:	PD Dr. rer. nat. Antje Ebert
Promotor-Vertretung:	Prof. Dr. mult. Thomas Meyer

Datum der mündlichen Prüfung: 26.01.2023

Hiermit erkläre ich, die Dissertation mit dem Titel "Characterization of the cytosolic and mitochondrial glutathione redox potential using cardiomyocyte specific transgenic Grx1-roGFP2 sensor mice" eigenständig angefertigt und keine anderen als die von mir angegebenen Quellen und Hilfsmittel verwendet zu haben.

Göttingen, den 17.01.2023 Andrea Fecke

Publication

Data of this thesis have been published in the following article:

Swain L, **Kesemeyer A**, Meyer-Roxlau S, Vettel C, Zieseniss A, Güntsch A, Jatho A, Becker A, Nanadikar MS, Morgan B (2016): Redox Imaging Using Cardiac Myocyte-Specific Transgenic Biosensor Mice. Circ Res 119, 1004–1016

Table of contents

List of Figures

List of Tables

List of Abbreviations

$E^{\circ\prime}_{GSH}$	glutathione midpoint redox potential under standard conditions
$E^{\circ\prime}_{roGFP2}$	roGFP2 midpoint redox potential under standard conditions
E_{GSH}	glutathione redox potential
E_{roGFP2}	roGFP2 redox potential
OxD_{GSH}	degree of oxidation of GSH
OxD_{roGFP2}	degree of oxidation of roGFP2
ΔE	potential difference
atp9	ATP synthase protein 9
BDM	2,3-Butanedione monoxime
bp	base pair
BSA	bovine Serum Albumin
CaMKII	Ca^{2+}/calmodulin-dependent kinase II
Blue CMAC	7-amino-4-chloromethylcoumarin
Complex I	NADH : ubiquinone oxidoreductase
Complex III	coenzyme Q : cytochrome c oxidoreductase
CVD	cardiovascular diseases
DTT	1,4-Dithiothreitol
ECC	excitation contraction coupling
EDTA	ethylenediaminetetraacetic acid
EF	ejection fraction
ER	endoplasmatic reticulum
FAS	fractional area shortening
G6PDH	glucose-6-phosphate dehydrogenase
GPX	glutathione peroxidase
Grx	glutaredoxin
GSH	glutathione
GSH_{total}	total concentration of GSH
GSNO	S-nitrosoglutathione
GSR	glutathione reductase
GSSG	glutathione disulfide
GST	glutathione s-transferase
HEPES	4-(2-Hydroxyethyl)-1-piperazineethanesulfonic acid
HPLC	high performance liquid chromatography
I/R	ischemia/reperfusion
MAO A	monoamine oxidase A
mBCl	monochlorobimane
MPTP	mitochondrial-permeability transition pore
MRC	mitochondrial respiratory chain
NADPH	nicotinamide adenine dinucleotide phosphate

nNT	nicotinamide nucleotide transhydrogenase
NOS	nitric oxide synthase
NOX	NADPH oxidase
Nrf2	nuclear factor erythroid 2 - related factor 2
PBS	phosphate buffered saline
PCR	polymerase chain reaction
PFA	paraformaldehyde
PKA	phosphokinase A
Prx	peroxiredoxin
RNS	reactive nitrogen species
roGFP2	reduction oxidation sensitive green fluorescent protein 2
ROS	reactive oxygen species
RyR2	ryanodine receptor 2
SERCA	sarcoplasmic/endoplasmic reticulum calcium ATPase
SOD	superoxide dismutase
Trx	thioredoxin
VEGF	vascular endothelial growth factor
wt	wild type
XO	xanthin oxidoreductase
α-MHC	α-myosin heavy chain
δ	dynamic range

1 Introduction

1.1 Redox homeostasis

The human organism is capable to preserve an internal balance against changing environmental conditions: body temperature, the cardiovascular system concomitant with fluid and electrolyte balance, pH value, and other parameters contributing to the maintenance of the cell's internal environment are kept constant to ensure optimal physiological functioning of the body. This stabilization of the internal state of equilibrium within a dynamic system is termed homeostasis.

One of these essential determinants of optimal cell activity is the homeostasis of the cellular redox status. It is generally described as a balance between oxidants and antioxidants. Oxidants are chemical molecules or compounds that act as electron acceptors and oxidize other substances. They include radical oxygen species (ROS), which are considered the major cause of oxidative stress (Cross et al. 1987). Starting from Denham Harman's theory in the 1950s that free radicals are related to the process of aging, oxidative stress is nowadays known to contribute to the pathophysiology of several diseases, including the broad spectrum of cardiovascular diseases (CVD) (Harman 1956; Zhang et al. 2007; Lee et al. 2017; Maritim et al. 2003; Burgoyne et al. 2012).

Antioxidants, which serve as electron donors and are thus oxidized, are commonly characterized with health-promoting and preventive properties. There have been attempts in studies to increase the availability of antioxidants to counteract the harmful effects of ROS. However, these efforts resulted both in beneficial and detrimental effects. (Jones 2006; Sharma et al. 2004)

Nowadays it is well known that redox signaling, a cellular signaling pathway via reactive species, contributes to the maintenance of physiological functions. The low-weight molecule glutathione (GSH) serves as an important cellular antioxidant along with multiple other metabolic functions and the GSH redox potential (E_{GSH}) is considered to reflect the cellular redox status (Schafer and Buettner 2001; Deponte 2017). Genetically encoded fluorescent redox probes exhibiting high affinity for GSH provide an excellent opportunity to achieve detailed subcellular analyses of the E_{GSH} (Meyer and Dick 2010).

Both oxidative stress and redox signaling are involved in cardiac physiology and pathology (Burgoyne et al. 2012; Santos et al. 2016). Therefore, it is of great interest to characterize the E_{GSH} of cardiomyocytes precisely to gain a more profound knowledge of the importance of E_{GSH} on cardiac intracellular processes and thus to have the ability to improve preventive and therapeutic strategies regarding cardiac pathologies.

1.2 Reactive species

The term ROS defines a group of free radicals (e. g., hydroxyl (HO·) and superoxide (O_2·-)) and reactive molecules (e. g., hydrogen peroxide (H_2O_2)) that contain oxygen and are characterized by their reactive behavior. Apart from exogenous causes as toxins, smoking, and ultraviolet and ionizing radiation, they are multiple endogenous cellular sources of ROS (Rahman et al. 2012; Jaimes et al. 2004). O_2·- is generated both nonenzymatically as a natural by-product in the mitochondrial respiratory chain (MRC) due to electron leakage of NADH : ubiquinone oxidoreductase (complex I) and coenzyme Q : cytochrome c oxidoreductase (complex III), and enzymatically by the membrane-bound nicotinamide adenine dinucleotide phosphate (NADPH) oxidases (NOX) via electron transfer from NADPH to O_2 (Bedard et al. 2007; Muller 2000). Major sources of H_2O_2 are superoxide dismutase (SOD) by catalyzing the dismutation of O_2·- as well as NOX4 (Fridovich 1989; Santos et al. 2016). The most reactive particle HO· is produced in presence of reduced transition metals like iron and H_2O_2 via the Haber-Weiss reaction (Michiels 2004; Lipinski 2011). With respect to the physiological purpose of ROS in cardiomyocytes, both the isoforms NOX2 and NOX4 are considered along with MRC to be the most important source (Burgoyne et al. 2012). However, NOX2 and NOX4 are related to the pathogenesis of various cardiac disease as well as xanthin oxidoreductase (XO), monoamine oxidase A (MAO A), and uncoupled nitric oxide synthase (NOS) are regarded as relevant sources of ROS in cardiac pathology (Minhas et al. 2006; Kaludercic et al. 2010; Burgoyne et al. 2012).

Apart from ROS, reactive nitrogen species (RNS) like nitric oxide (NO) and its derivatives, e. g. peroxynitrite ($ONOO^-$), are regarded as another reactive species of great biological importance (Dröge 2002). NO is synthesized via three isoforms of NOS, of which the endothelial and neuronal NOS are present in cardiomyocytes under physiological conditions whereas expression of inducible NOS is upregulated during inflammation (Brown and Borutaite 2007; Infante et al. 2021). The existence of a specific mitochondrial NOS isoform remains controversial (Poderoso et al. 2019; Lacza et al. 2009). In presence of O_2^- - NO reacts nonenzymatically to $ONOO^-$, a much more potent oxidant to which the deleterious effects of NO are ascribed (Pacher et al. 2007).

A significant increase of both ROS and RNS, exceeding the antioxidant capacity of the cell, results in damage to various structures including DNA, proteins, and lipids leading to dysfunction and subsequent apoptosis of the cell (Slater et al. 1995; Pacher et al. 2007). The imbalance between oxidative and reductive components in favor of oxidants due to ROS, leading to physiological malfunction and cellular damage, is termed oxidative stress (Sies 2015; Jones 2006). Similarly, the increased and uncontrolled generation of RNS is called nitrosative stress (Klatt and Lamas 2000).

1.3 Redox Signaling

Throughout many years, research has focused on the harmful, pathological effects of ROS in the context of oxidative stress. Starting around the beginning of the 21st century, the signaling effect of reactive species in physiological processes became increasingly important. The oxido-reductive processes in redox signaling can be characterized simplified by reversible reactions, which occur in a temporally and spatially limited environment, instead of irreversible, uncontrolled effects as in oxidative stress (Forman et al. 2004; Kaludercic et al. 2014). Subcellular, organellar compartments such as the endoplasmatic reticulum (ER), mitochondria as well as the cytosol represent such defined areas, which were shown to differ in their redox environment (Go and Jones 2008). This will be discussed in more detail in section 1.5.2.

Due to its functional thiol group and its characteristic to be the most nucleophilic side chain in the physiological environment, the amino acid cysteine (Cys) is regarded as the most important target structure of redox signaling (Lo Conte and Carroll 2013). Its tendency to react with reactive species is dependent on the pKa of the related thiol group, which is significantly influenced by its microenvironment within the proteins and enzymes (Poole 2015). As described by Forman et al. (2014), this emphasizes that not the sheer abundance of Cys but their specific localization within molecular structures turns them into redox signaling targets. The formation of inter- or intramolecular disulfides induces modifications of the three-dimensional configuration, which results in activation or inactivation of enzymes as well as binding characteristics of molecules involved in signaling pathways may be affected (Winterbourn and Hampton 2008; Lo Conte and Carroll 2013). However, in the absence of nearby thiols (e. g. GSH) or amides and the presence of high concentrations of reactive species, irreversible oxidation products are generated (Poole 2015; Klomsiri et al. 2011).

H_2O_2 is considered the most relevant ROS in redox signaling as it fulfills various criteria to function as a signal molecule (Sies 2017). Both its enzymatic and local production via SOD and NOX enzymes and its removal via peroxidases, peroxiredoxins (Prx) and other cellular antioxidant defense systems including the GSH system, enable transient increases and thus provide spatial and temporal specificity concerning target structures nearby (Forman et al. 2014). The free radical NO is known to be involved in physiological processes, such as the well-known vasodilatory effect, where binding of NO leads to an increase of cyclic guanosine monophosphate (cGMP) levels (Underbakke et al. 2014). Moreover, like H_2O_2, NO may lead to posttranslational modifications of proteins via interaction with Cys by S-nitrosylation or tyrosine nitration (Forman et al. 2014). In addition, both oxidative and nitrosative stimuli may result in S-glutathionylation of Cys, the formation of a mixed disulfide between protein thiols and GSH, which is regarded, similar to phosphorylation, as a signal transduction mechanism in proteins (Mieyal et al. 2008; Musaogullari and Chai 2020). S-glutathionylation can be mediated via S-nitrosoglutathione (GSNO), a conjugate of NO and GSH, which is regarded as a central part in NO signaling (Broniowska et al. 2013).

Furthermore, along with glutathione S-transferase (GST), the small redox proteins glutaredoxins (Grx) are involved in redox signaling as important mediators of S-glutathionylation (Matsui et al. 2020). Grx is a small redox enzyme belonging to the Thioredoxin (Trx) fold family, and exhibiting a special affinity for GSH (Aquilano et al. 2014). It is attributed a crucial role in the de-/glutathionylation of mixed disulfides with proteins, which alters protein function (Lillig et al. 2008).

Regarding redox signaling, GSH is not only indirectly involved as an antioxidant in the defense against oxidative and nitrosative stress to maintain redox homeostasis but directly plays an important role as an adduct of Cys in signaling mechanisms in cellular processes influenced by the cellular redox state (Aquilano et al. 2014).

1.4 The impact of reactive species in cardiac health and disease

Both ROS and RNS are of importance in cardiomyocytes within physiological processes as well as the development of pathologies (Pacher et al. 2007; Burgoyne et al. 2012). Since mitochondria, representing both the regeneration of adenosine triphosphate (ATP) and a potential source of ROS, constitute about one third of the cellular volume of cardiomyocytes, the maintenance of the cellular redox homeostasis is challenging (Christians and Benjamin 2012). Starting with the involvement of redox signaling in cell differentiation and proliferation of cardiomyocytes, several cardiac enzymes and proteins are now known redox targets of ROS and RNS that play a significant role in excitation-contraction coupling (ECC) or are important for the metabolic function of the cell (**Figure 1**) (Burgoyne et al. 2012; Santos et al. 2016; Hare 2004).

ROS contribute to the maintenance of intracellular calcium (Ca^{2+}) levels and thus cardiomyocyte contractility (Sag et al. 2013). The ryanodine receptor 2 (RyR2), mediating the Ca^{2+}-induced Ca^{2+} release, is oxidized by ROS produced via NOX2, which is activated via stretch and localized to the membrane of t-tubules (Prosser et al. 2011). Likewise, activation of neuronal NOS has been shown to increase RyR2-activity through S-nitrosylation (Wang et al. 2010). In addition, oxidation of cyclic adenosine monophosphate (cAMP) dependent protein kinase (PKA), phosphorylating several proteins involved in ECC, is increased cAMP independently both in its catalytic activity and binding characteristics to A-kinase anchoring proteins due to formation of two interprotein disulfides (Brennan et al. 2006; Santos et al. 2016). By generating a mouse model in which oxidation of PKA is inhibited by mutation of the corresponding Cys, Burgoyne et al. (2015) demonstrated that oxidation of PKA, presumably via ROS generated by NOX4, has a significant role in vascular endothelial growth factor (VEGF) induced signal transduction pathway of angiogenesis involving the extracellular signal-regulated kinase and the cAMP responsive element binding protein (ERK/CREB pathway). Additional identified redox-regulated cardiac proteins of the ECC include cGMP-dependent protein kinase G, cardiac SR Ca^{2+}-ATPase (SERCA),

Ca^{2+}/calmodulin-dependent kinase II (CaMKII), and further enzymes located downstream of PKA and CamKII (Burgoyne et al. 2012).

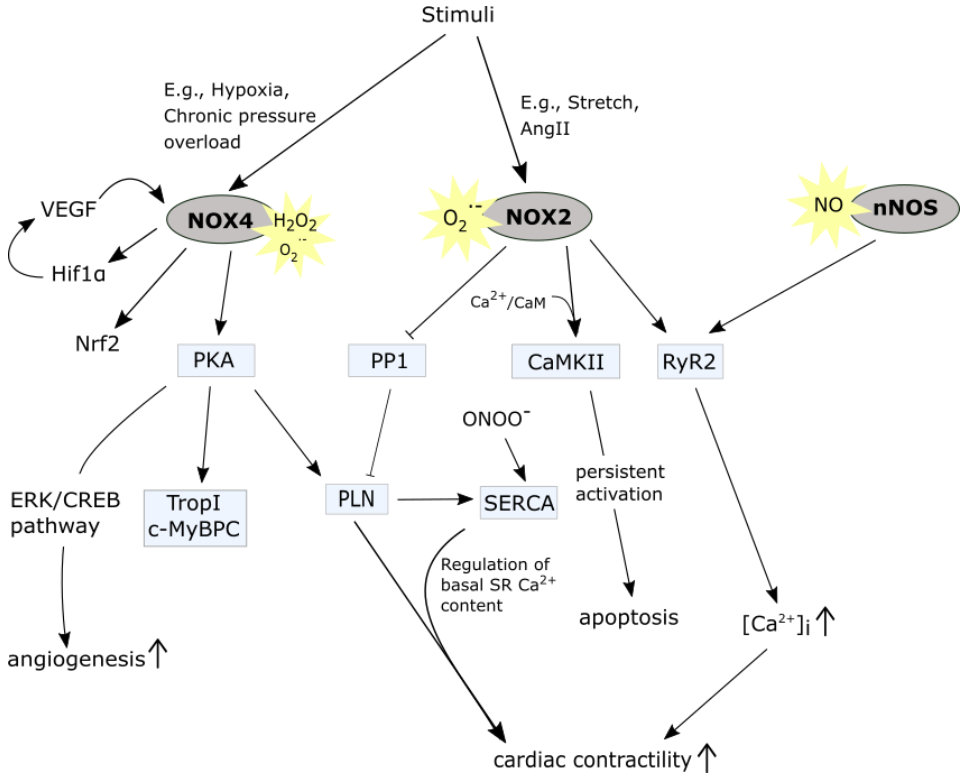

Figure 1: Redox signaling in cardiomyocytes. Examples of redox signaling in cardiomyocytes as described in the literature. NADPH oxidases (NOX) 2 and 4 and neuronal nitric oxide synthase (nNOS) generate O2-, H_2O_2, and NO, respectively, which modulate enzymes. proteins, and channels of the excitation-contracting coupling as well as they are in involved in apoptosis (NOX2), regulation of Nrf2 (nuclear factor erythroid 2 – related factor 2) and angiogenesis (NOX4). ┤ indicates inhibtion and ▶ activation. VEGF: vascular endothelial growth factor, Hif-1α: hypoxia inducible factor 1 α, PKA: phosphokinase A, PP1: protein phosphatase 1, CaMKII: Ca^{2+}/calmodulin-dependent kinase II, RyR2: ryanodine receptor 2, Trop I: Troponine I, c-MyBPC: cardial myosin binding protein c, PLN: phospholamban, SERCA: Sarcoplasmic/endoplasmic reticulum calcium ATPase, ERK: extracellular signal-regulated kinase, CREB: cAMP responsive element binding protein, SR: sarcoplasmatic reticulum, $[Ca^{2+}]i$: intracellular Ca^{2+} concentration.

Regarding the redox regulation of metabolic enzymes, Eaton et al. (2002) have shown that in cardiomyocytes several proteins are S-glutathionylated during reperfusion after ischemia, in particular glyceraldehyde-3-phosphate dehydrogenase, an important enzyme of glycolysis that catalyzes the reaction of glucose-3-phosphate to 1,3-biphosphoglycerate. S-glutathionylation at the active site reduces the activity of the enzyme (Dalle-Donne et al. 2009). Ralser et al. (2007) consider this inhibition as a change in metabolism of carbohydrates from glycolysis to the pentose-phosphate pathway, an essential pathway for the formation of NADPH, the cofactor for the maintenance of antioxidant systems.

With respect to the development of cardiac pathologies, ROS have long been considered as a critical factor. By the 1980s, oxidative stress had been linked to the pathogenesis of

ischemia/reperfusion (I/R) injury (Guarnieri 1980). The main sources of ROS during I/R injury are mitochondrial respiratory chain, NOX, XO, and MAO enzymes (Kinugasa et al. 2003; Zhou et al. 2015; Chen and Zweier 2014). The generation of mitochondrial ROS has been attributed an important role, as they may lead both to damage of mitochondrial DNA with subsequent functional impairment of the respiratory chain and to the opening of the mitochondrial-permeability transition pore (MPTP) (Perrelli et al. 2011; Lakshmi et al. 2009). Subsequently, this results in the collapse of the mitochondrial membrane potential, leading to the release of cytochrome c and thus to the induction of apoptosis (Borutaite 2003). Furthermore, an increased NO production due to expression of inducible NOS after myocardial infarction was shown to contribute to myocardial dysfunction (Feng et al. 2001).

Apart from the pathogenesis of I/R-injury, NOX enzymes have been shown to be associated with the development of heart failure, cardiac remodeling, and cardiac hypertrophy (Heymes et al. 2003; Nakagami 2003; Looi et al. 2008). According to Morawietz (2018), the precise function of NOX4 has not yet been completely understood. A study by Kuroda et al. (2010) showed a better outcome of cardiac function in pressure overload in cardiac-specific NOX4-knockout-mice, but other studies postulated a protective role of NOX4. Zhang et al. (2010) and Smyrnias et al. (2015) demonstrated an activation of Hif-1α, release of VEGF, and activation of the cytoprotective transcription factor nuclear factor erythroid 2 - related factor 2 (Nrf2) via NOX4 during chronic pressure overload.

Thus, the balance of ROS and RNS in the physiology and pathology of cardiomyocytes is of great importance, since redox signaling needs to be allowed, but oxidative stress should be avoided. The glutathione redox couple (2GSH/GSSG) plays an important role in regulating the cellular redox state, which turns it into an interesting subject for further investigations to gain a better understanding of physiological and pathophysiological redox mechanisms in cardiomyocytes.

1.5 Glutathione (GSH)

GSH, formally L-γ-glutamyl-L-cysteinylglycine, is an atypical tripeptide, which represents one of the most important antioxidant substances in all somatic cells. One of the main function of the low-molecular weight thiol is to maintain the cellular and subcellular redox status of thiols (Ballatori et al. 2009). GSH is exclusively synthesized in the cytosol but is also present in other cell compartments, such as the mitochondria, the ER or nucleus (Forman et al. 2009). The function of GSH derives in particular from the highly nucleophilic thiol group of Cys, which is able to form various bonds with other molecules (Couto et al. 2016). Besides its function of maintaining the cellular and subcellular redox status of thiols, GSH serves as a cofactor of the GST in the second phase of xenobiotic biotransformation. In addition, the GSH pool serves as a reserve for the amino acid cysteine and is essential for the regeneration of other antioxidants such as ascorbic acid and vitamin E (Meister 1988; Winkler et al. 1994). Regarding redox signaling, GSH is of great importance both indirectly

as a co-factor via the GSH-dependent oxidant defense system, and directly in S-glutathionylation, the formation of a mixed disulfide between GSH and a protein, as well as the reaction of GSH with NO to form GSNO (Zhang and Forman 2012; Aquilano et al. 2014).

1.5.1 GSH redox cycle and regulation of GSH

As the major non-enzymatic antioxidant of cellular redox maintenance, GSH not only directly scavenges radical forms of reactive species (e. g. HO· and ONOO-) but is also involved indirectly as a cofactor in the reduction of protein thiol groups and the detoxification of peroxides (**Figure 2**). In particular, this is mediated by GSH-dependent peroxidases (GPX), which eliminate peroxides such as H_2O_2 and peroxynitrous acid (ONOOH), oxidizing two monomers of GSH as reducing equivalents to GSSG (Lu 2013; Sies et al. 1997; Hanschmann et al. 2013). Regeneration of GSH from GSSG is driven NADPH-dependent via the enzyme glutathione reductase (GSR), which is present in cytoplasm as well as in organelles like mitochondria and the nucleus (Couto et al. 2016). The regeneration of NADPH occurs via the pentose phosphate pathway by glucose-6-phosphate dehydrogenase (G6PDH), which was shown to be critical for maintaining cytosolic GSH of cardiomyocytes to avoid dysfunction due to decreased resistance against radicals and disturbance of intracellular calcium transport (Jain et al. 2003). In mitochondria, however, NADPH is regenerated independently by nicotinamide nucleotide transhydrogenase (nNT), isocitrate dehydrogenase 2 (IDH2), and decarboxylating malic dehydrogenase (dMD) (Nickel et al. 2015).

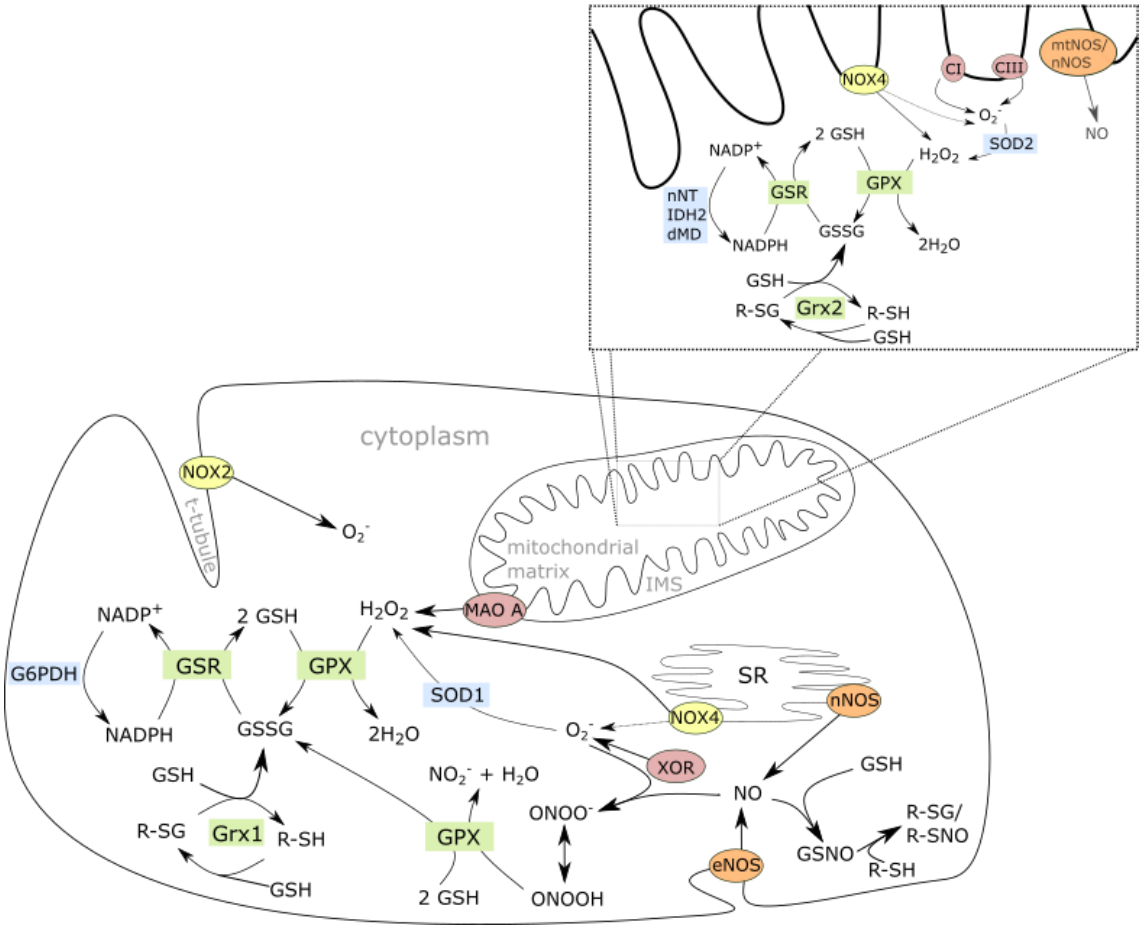

Figure 2: The GSH redox cycle and sources of ROS/RNS in cardiomyocytes. Overview of the redox active enzymes and ROS/RNS as well as the GSH redox cycle in both cytoplasm and mitochondrial matrix. NOX (NADPH oxidase) 2 and NOX4 (yellow) represent along with other enzymes (red) the major sources of ROS in cardiomyocytes, whereas nNOS (neuronal nitric oxide synthase) and eNOS (endothelial NOS) (orange) are major physiological sources of NO. O_2- is dismutated via SOD 1/2 (superoxide dismutase 1/2; blue) to H_2O_2, which is scavenged via the GSH dependent redox system (green), among others. The co-factor NADPH is regenerated in the cytoplasm and mitochondrial matrix via G6PDH (glucose-6-phosphate dehydrogenase) or nNT (nicotinamide nucleotide transhydrogenase), IDH2 (isocitrate dehydrogenase 2), and dMD (decarboxylating malic dehydrogenase), respectively. Upon reaction of NO with GSH GSNO (S-nitrosoglutathione) is formed, which may lead to S-nitrosylation (R-SNO) and S-glutathionylation (R-SG). As well, $ONOO^-$ (peroxynitrite) is formed via the reaction of NO with $O2^-$. GPX: glutathione peroxidase, GSR: glutathione reductase, Grx1/2: glutaredoxin1/2, MAO A: monoamine oxidase A, XOR: xanthine oxidoreductase.

Apart from GSR maintaining the reducing GSH pool, the 2GSH/GSSG is as well modulated by *de novo* synthesis and export of the low-weight molecule (Deponte 2017). GSH is synthesized in two ATP-dependent steps from the three amino acids L-glutamic acid, L-cysteine, and glycine via the enzymes glutamate cysteine ligase (GCL) and glutathione synthetase (GS) (Lu 2013). The formation of γ-glutamylcysteine by GLC is regarded apart from the intracellular availability of L-cysteine as a limiting step in the synthesis of GSH, which in turn modulates the activity of GLC via feedback inhibition (Dalton et al. 2004;

Richman and Meister 1975). Both during basal conditions and increased oxidative stress, GLC expression and thus the total GSH concentration (GSH_{total}) is pre-translationally induced by transcription factors including Nrf2, NkappaB, and AP1 (Meng et al. 2010; Wild et al. 1999; Rahman et al. 1998; Lu 2013). GSH_{total} as well as the GSH:GSSG ratio is influenced by the extracellular export of GSH and/or GSSG, which most likely involves the multidrug-resistance protein (MRP) family and transporters of the organic anion transporting polypeptide (OATP) family (Ballatori et al. 2005). Due to the atypical γ-glutamyl peptide bond, GSH is highly stable against degradation by regular peptidases and proteases (Bajic et al. 2019). The degradation of GSH via hydrolysis of the peptide bond between γ-glutamyl and cysteine occurs extracellularly by γ-glutamyltranspeptidase (GGT) bound to the plasma membrane of epithelial cells, and is followed by hydrolysis of cysteinylglycine via dipeptidases, releasing cysteine for intracellular GSH synthesis (Lu 2009; Ballatori et al. 2009).

1.5.2 GSH and redox compartmentalization

The maintenance of the redox status should not be seen as a global condition of the entire cell: there is evidence that the individual subcellular compartments differ in their redox states and the different cellular redox pairs are also in non-equilibrium within these compartments (Jones and Go 2010). This is described as redox compartmentalization. Along with 2GSH/GSSG, especially Trx-SH/Trx-SS (a redox couple of the Trx fold family, which acts in its reduced form GSH-independent as an oxidoreductase) and NADP+/NADPH are of particular importance (Aquilano et al. 2014). A prominent example of redox compartmentalization is the specific signaling via the epidermal growth factor (EGF) (Halvey et al. 2005): Exposition to exogenous oxidants leads to general oxidation of thiol-disulfide redox couples, but upon activation of the EGF receptor (EGFR), the redox potential of the cytosolic isoform of Trx was increased about 20 mV. However, nuclear and mitochondrial Trx remained unaffected as well as the redox state of cellular GSH remained unchanged, which indicates that physiological effects may take place due to specific regulated signaling mechanisms.

The redox couple 2GSH/GSSG is regarded as the most relevant cellular redox buffer. Hence, E_{GSH} is constantly referred to as a useful indicator of the cellular redox status as it reflects the reducing capacity of the related redox couple (Schafer and Buettner 2001; Jones 2002). Changes in E_{GSH} have a pivotal role in cellular processes within physiological conditions, thus the maintenance of the intracellular and intracompartmental redox status of 2GSH/GSSG is of great importance concerning the defense against oxidative stress as well as the regulation of redox signaling (Lu 2013; Aquilano et al. 2014).

E_{GSH} is described by the Nernst equation, which allows an estimation of the reduction potential of the related redox couple:

$$E_{GSH} = E^{\circ\prime}_{GSH} - \frac{RT}{2F} \ln\left(\frac{[GSH]^2}{[GSSG]}\right)$$

R is the gas constant, T the absolute temperature, and F the Faraday constant. $E^{\circ\prime}_{GSH}$ is the midpoint redox potentials under standard conditions ($T = 298.15\ K, pH = 7.0$), which was determined to be -240 mV. (Schafer and Buettner 2001)

Compared to other cellular redox buffers (e. g. Trx-SH/Trx-SS, which forms an intramolecular disulfide), E_{GSH} depends in addition to the ratio of the reduced to the oxidized also on the absolute concentration of GSH_{total}, since two molecules of GSH are oxidized to one molecule of GSSG (GSH_{total} = [GSH] + 2[GSSG]) (Meyer and Dick 2010).

The concentration of GSH, the GSH:GSSG ratio and the regulation of 2GSH/GSSG vary within different subcellular compartments (Christians and Benjamin 2012). Through the application of specifically targeted fluorescent redox sensors, it has been previously demonstrated in *Saccharomyces cerevisiae*, *Drosophila melanogaster* and HeLa cells, among others, that the cytoplasm and mitochondrial matrix exhibit different GSH redox pools (Braun et al. 2010; Morgan et al. 2011; Østergaard et al. 2004; Albrecht et al. 2011; Dooley et al. 2004; Hanson et al. 2004). Similarly, conventional measurements for GSH indicated the existence of different redox compartments as well, but the advantages of GFP-based sensors will be discussed in Section 1.6.3 (Jones and Go 2010; Rebrin et al. 2003).

The majority of GSH_{total} is located in the cytoplasm (> 80 %) (Schafer and Buettner 2001; Meister and Anderson 1983; Lu 2013). The cytosolic GSH:GSSG ratio was shown to vary with the cellular functional state within differentiation, proliferation, and apoptosis (Kirlin et al. 1999; Jones and Go 2010). As the cytoplasm exhibits rarely metabolic oxidases compared to other organelles (e. g. mitochondria), Go and Jones (2008) suggest it as both a bufferzone between other redox active organelles and a medium, where specific and sensitive ROS and RNS signaling via NOX and NOS can take place. The cytoplasm of the cardiomyocytes is characterized particularly by the myofilaments, being present as a highly organized and structured contractile apparatus, as well as by the enzymes and channels involved in the ECC and Ca^{2+} homeostasis (Santos et al. 2011; Christians and Benjamin 2012). Both contribute to cardiac contractility and are subject to redox regulation (Santos et al. 2011). However, until the time of our study, there was no mouse model that allowed the dynamic, reversible, and specific measurement of cytosolic E_{GSH}, which is of particular interest regarding the involvement of redox signaling events in essential cardiac functions.

The mitochondria contain the second most part of the GSH_{total} with up to 15%, while only a minor part is localized in other subcellular compartments (e. g. ER and nucleus) (Meister and Anderson 1983; Lu 2013). Since GSH is exclusively synthesized in the cytoplasm, the mitochondrial GSH concentration relies on transport of GSH via mitochondrial dicarboxylate and the 2-oxoglutarate carrier (Chen and Lash 1998; Wilkins et al. 2013). Mitochondria represent about a third of the cellular volume of cardiomyocytes and are of

particular importance, as they are involved in the regulation of intracellular Ca^{2+} signaling and apoptosis and, furthermore, are a major source of ROS due to the MRC and are simultaneously highly sensitive to oxidative stress (Jones and Go 2010). Various mitochondrial proteins were shown to be regulated via S-glutathionylation, e. g. the complexes of MRC localized at the inner mitochondrial membrane (Mailloux et al. 2014a; Wang et al. 2013; Hurd et al. 2008; Chen et al. 2007). In addition, Aon et al. (2007) demonstrated that changes in the ratio of GSH:GSSG and the total amount of GSH in cardiomyocytes have an influence on the opening of the inner membrane anion channel and MPTP. Measurements of mitochondrial GSH used to be challenging as conventional methods required isolation of mitochondria which may result in loss and artificial oxidation of GSH, but the development of genetically encoded biosensors provide new specifically targeted tools to determine the mitochondrial E_{GSH} (Go and Jones 2008; Calabrese et al. 2017).

1.6 The Grx1-roGFP2 sensor

1.6.1 Reduction-oxidation sensitive GFP2 (roGFP2)

The reductions-oxidation sensitive GFP2 (roGFP2) is derived from GFP which was discovered and extracted from jellyfish *Aequorea victoria* by Osamu Shimomura in 1962 (Shimomura et al. 1962). Since Chalfie et al. (1994) showed that expression of GFP in prokaryotic and eukaryotic cells exhibit the same fluorescent characteristics as in A*equorea victoria*, genetically encoded GFP were applied for specific detection of genes and proteins (Cinelli et al. 2000). GFP is a soluble protein of 27 kDa consisting of 238 amino acids (Meyer and Dick 2010). The structure of GFP is characterized by a barrel through 11 β-strands with an α-helix running interiorly along the axis of the β-barrel (Ormö et al. 1996; Yang et al. 1996a). The fluorescent properties of GFP are given via the three amino acids Ser 65, Tyr 66, and Gly 67, which form an p-hydroxybenzylideneimidazolinone chromophore through post-translational intramolecular cyclization, dehydration, and oxidation leading to a conjugated system of π-electrons, which are able to absorb and emit visible light via uptake and subsequently release of energy (Tsien 1998; Meyer and Dick 2010; Cannon and Remington 2008). Depending on whether the phenol group of Tyr 66 is present in a protonated neutral or deprotonated anionic form, GFP is excited at either 395 nm or 475 nm, respectively (Brejc et al. 1997; Elsliger et al. 1999). However, due to the phenomena of excited state proton transfer, in which a proton of Tyr 66 is transferred to Glu 222, there is only one emission peak at 509 nm (**Figure 3**) (Chattoraj et al. 1996; Meech 2009).

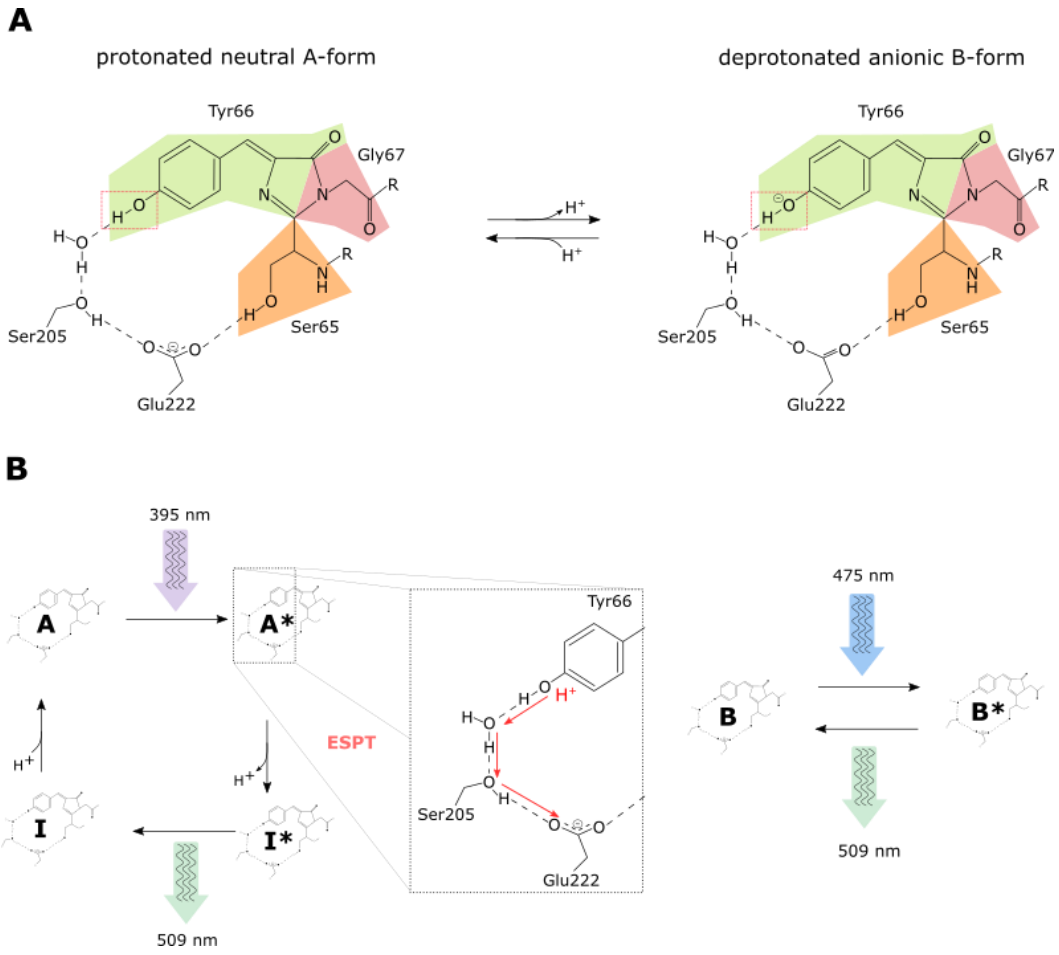

Figure 3: Protonation state of the chromophore of wildtype GFP. (A) The chromophore of wt (wild type) GFP, which is formed via the three amino acids Ser65 (orange), Tyr66 (green) and Gly67 (red), is characterized by the protonation state of phenol group (red box) of Tyr66. Changes of protonation state involves an H-bonding network, which include Ser205, Glu222 and a structural H_2O molecule. Modified from Meyer and Dick (2010), courtesy of Mary Ann Liebert, Inc. **(B)** In the deprotonated anionic B-form GFP is excited at 475 nm to its excited form B* and emits light at 509 nm. However, after excitation of the protonated neutral A-form at 395 nm, the emitted light is also 509 nm. This property is due the phenomena of excited state proton transfer (ESPT), in which the proton of the phenol group of Tyr66 is transferred to a carboxylate of Glu222 (red arrows). The excited A-form (A*) is transferred via ESPT to an excited intermediate form (I*), which then emits light at 509 nm and is transferred to the relaxed I-form. The I-form is returned to the relaxed A-form via protonation of the phenol group. Modified from Chattoraj et al. (1996), courtesy by National Academy of Sciences, U. S. A. Copyright (1996) National Academy of Sciences, U. S. A.

Individual modifications of the amino acids of GFP may influence the chromophore and its protonation state. Enhanced GFP (eGFP) results from the substitution of Ser65 by Threonin (S65T mutation) and Phe64 by Leu (F64T mutation) which lead to favored depronotation of the chromophore directing the major exciation peak to 488 nm with improved fluorescent brightness (Yang et al. 1996b; Heim et al. 1995).

RoGFP2 was developed by Hanson et al. (2004), who substituted S147 and Q204 with Cys at the β-barrel strands 7 and 10 of the eGFP (**Figure 4**). The excitation maxima remained

unchanged, however, the formation of a disulfide bridge results in minor structural changes near the chromophore, so that the protonated status of Tyr66 is preferred (Hanson et al. 2004). As a result, compared to reduced roGFP2 (roGFP2$_{red}$), the excitability of oxidized roGFP2 (roGFP2$_{ox}$) is increased at 405 nm and decreased at 488 nm. 405 nm and 488 nm represent standard laser wavelengths, corresponding either exactly or approximately to the excitation maxima of roGFP2. The fluorescence intensity ratio of the emission at 510 nm after excitation with 405 nm and 488 nm (I405/488) therefore serves as a useful tool to reflect the oxidation state of the roGFP2.

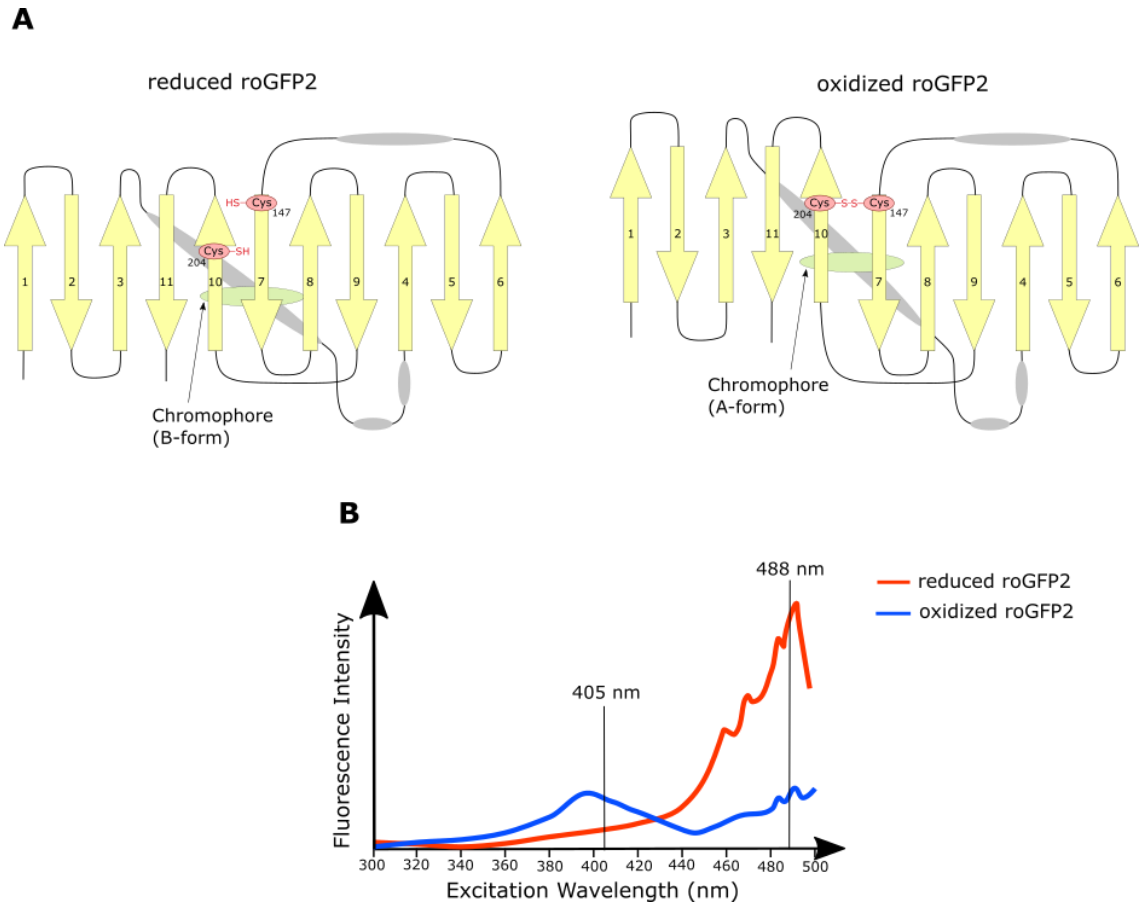

Figure 4: Schematic structure and fluorescence intensity of roGFP2. (A) The structure of roGFP2 contains 11 antiparallel β strands, which form a barrel in which the chromophore is localized. Oxidation of the two engineered Cys at position 204 and 147 leads to the formation of a disulfide bond and conformational changes, so that the protonated A-form is favored. Based on and modified from Aller et al. (2013), licensed under CC BY 3.0 (https://creativecommons.org/licenses/by/3.0/). **(B)** The fluorescence intensity of roGFP2 is shown in dependence on the excitation wavelength. In the deprotonated B-form (reduced roGFP2, red curve) the maximum of excitability is reached at 490 nm, whereas in the protonated A-form (oxidized roGFP2, blue curve) the maximum is reached at 400 nm. The maxima are close to the standard laser wavelength 405 and 488 nm (black lines). Modified from Meyer and Dick (2010), courtesy of Mary Ann Liebert, Inc.

The midpoint potential of roGFP2 ($E^{\circ\prime}_{roGFP2}$) was determined to be -280 mV (Hanson et al. 2004; Dooley et al. 2004). $E^{\circ\prime}_{roGFP2}$ is significantly more negative than the midpoint potential of GSH ranging from -151 to -181 mV depending on the concentration of GSH_{total} upon physiological conditions. Thus, roGFP2 represent a very well suited sensor to detect even small changes in the E_{GSH}. (Meyer and Dick 2010)

1.6.2 Substrate and compartment specificity of roGFP2

Studies by Meyer et al. (2007) and Schwarzländer et al. (2008) have shown that roGFP2, although not exclusively, interacts predominantly with 2GSH/GSSG. The roGFP2 represents an artificial substrate of Grx that mediates the equilibrium between roGFP2 and the cellular GSH pool. The rate constant of uncoupled roGFP2 is however too slow to reflect oxidative changes either of short duration or minor changes in the total E_{GSH} as they rely on the present intracellular Grx pool (Cannon and Remington 2008). Gutscher et al. (2008) therefore developed a fusion protein of human Grx1 and roGFP2 to improve the specificity and speed of the sensor to allow real time imaging. Gallogly et al. (2009) showed that the fusion increases the local Grx1 concentration at the roGFP2-sensor by about three orders of magnitude.

As an artificial substrate of Grx1, roGFP2 can be both glutathionylated and deglutathionylated via a monothiol ping-pong mechanism (**Figure 5**) (Meyer et al. 2007; Gutscher et al. 2008; Schwarzländer et al. 2016): When E_{GSH} increases above the redox potential of roGFP2 (E_{roGFP2}), formation of an intramolecular disulfide at roGFP2 occurs via the intermediate step of a mixed disulfide with GSH until an equilibrium between E_{GSH} and E_{roGFP2} is established. The intramolecular disulfide bond leads to conformational changes of roGFP2 and its fluorophore resulting in altered excitation behavior. Once E_{GSH} decreases and $E_{GSH} < E_{roGFP2}$, this process occurs in revers to maintain $E_{GSH} = E_{roGFP2}$. For instance, an increase in E_{GSH} may be due to increased H_2O_2 levels buffered by the GSH system. According to Meyer and Dick (2010), the reaction mechanism of Grx1-roGFP2 and GSH exemplifies how signal transduction in redox signaling is mediated via Grx or similar redox enzymes (e. g. Trx).

Apart from the specificity for the 2GSH/GSSG redox pair, the GFP-based redox sensors also feature high specificity for the various subcellular compartments such as the mitochondrial matrix, intermembrane space, ER, and nucleus by applying specific targeting sequences (Kostyuk et al. 2020). Such specific localization of the sensor is ideal to study E_{GSH} within distinct subcellular compartments without destroying the cell, allowing dynamic measurements within these compartments as well.

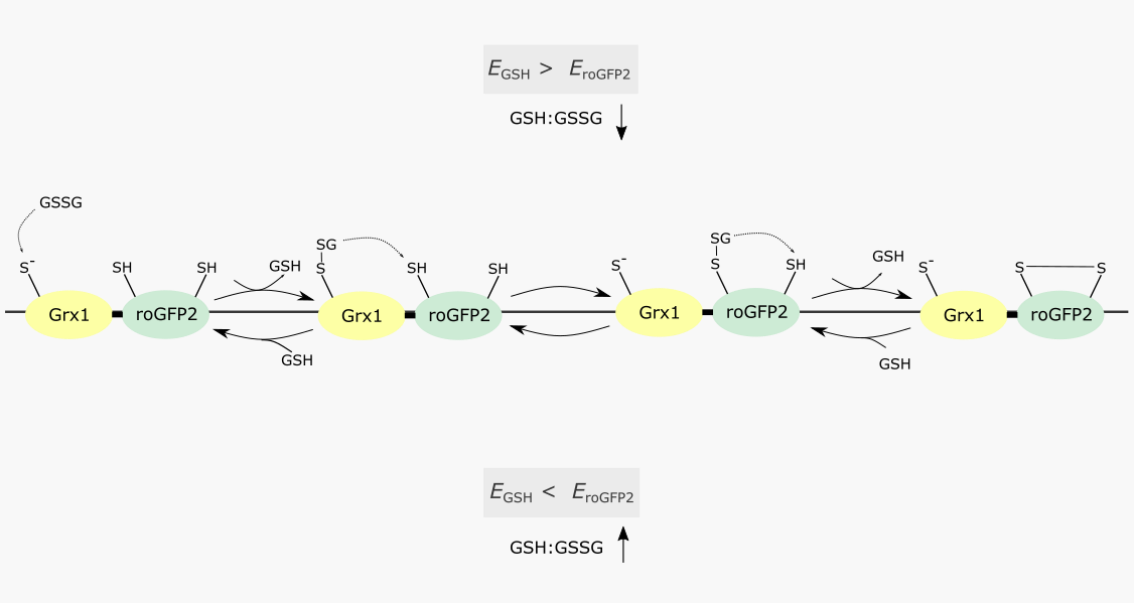

Figure 5: Scheme of the equilibration of Grx1-roGFP2 and GSH. Upon oxidizing conditions, GSSG rises and $\boldsymbol{E_{GSH}}$ (glutathione redox potential) becomes more oxidized than $\boldsymbol{E_{roGFP2}}$ (roGFP2 redox potential). The monothiol group of Grx1(glutaredoxin 1), present as a thiolate (-S-), attacks one of the sulfurs of GSSG and forms Grx1-SSG with release of GSH. Grx1-SSG then reacts with one of the Cys resdiues of roGFP2, which forms subsequently an intramolecular disulfide bond with release of GSH. This mechanism happens in reverse at the expense of GSH when $\boldsymbol{E_{roGFP2}}$ is more oxidized than $\boldsymbol{E_{GSH}}$. Modified from Meyer and Dick (2010), courtesy of Mary Ann Liebert, Inc.

1.6.3 Comparison with conventional methods for the determination of GSH

Prior to the development of the roGFP variants, there were and still are other methods used to determine the intracellular GSH content and the ratio GSH:GSSG. Among these conventional methods, the group of high performance liquid chromatography (HPLC), spectrophotometry, and fluorometry can be distinguished from the redox sensitive dyes (Pastore et al. 2003).

The former measurement methods are based on the derivatization of GSH, which results in a GSH product that is photometrically detectable, with HPLC being the most frequently used (Pastore et al. 2003; Forman et al. 2009). Indeed, these methods achieve high specificity for both reduced and oxidized GSH, but the destruction of the cellular structures eliminates any information about compartment-specific characteristics, as well as artificial oxidation cannot be excluded, and dynamic measurements are impossible (Meyer and Dick 2010; Kaludercic et al. 2014).

Although the measurement of GSH using redox-sensitive fluorescent dyes requires no destruction of the cell, they are mostly characterized by irreversible reactions and lack of specificity concerning the compartments and the redox couple 2GSH/GSSG (Meyer and Dick 2010; Dooley et al. 2004). Some redox sensivite dyes (e. g. 7-amino-4-chloromethylcoumarin (Blue CMAC) and monochlorobimane (mBCl)) apparently have a

higher affinity for GSH but not exclusively (Tauskela et al. 2000). Another concern with redox sensitive dyes is the effect of photobleaching, affecting the signal intensity, and thus potentially leading to mismeasurements (Eggeling et al. 1998).

Due to the ratiometric measurement with the Grx1-roGFP2 sensor, effects due to photobleaching, low sensor expression and changes of pH are minimized (Hanson et al. 2004; Schwarzländer et al. 2016). The specificity of roGFP2 towards the 2GSH/GSSG redox couple is given by the fusion with Grx1 as described above. However, it was additionally shown that roGFP2 in general does not interact with Trx (Gutscher et al. 2008). Among the significant advantages of Grx1-roGFP2 compared with conventional methods is its specific subcellular localization, which allows the analysis of E_{GSH} in a compartment-specific manner. Furthermore, the fusion to Grx1 and the reversible reaction with GSH allows a dynamic measurement both *ex vivo* and *in vivo*, so that not solely a static value of E_{GSH} but its alteration under different conditions can be monitored (Gutscher et al. 2008).

Compared to another genetically encoded redox sensor, a redox sensitive derivation of the yellow fluorescent protein (rxYFP), roGFP variants benefit from their ratiometric behavior, since YFP exhibits just a single fluorescence excitation peak, whose signal emission amplitude changes upon formation of the disulfide bond (Hanson et al. 2004; Cannon and Remington 2008).

The other variant of roGFP, namely roGFP1, shows as well a ratiometric behavior, but in comparison to roGFP2 it exhibits a reduced brightness and the effect of photoswitching to a variant with different spectral properties at high irradiation at 405 nm (Schwarzländer et al. 2008).

1.7 Aim of this thesis

Cardiomyocytes are essential as a functional syncytium for the contractility and function of the heart. Regulated processes are required to ensure that the individual cells act collectively as a unified entity. An important factor contributing to optimal cardiac function is the maintenance of the redox homeostasis. Various cardiac enzymes are subject to redox-regulated control, and dysregulation of redox balance has been associated with diverse pathologies such as I/R injury, heart failure and hypertrophy. The total cellular redox status as well as the redox status of the subcellular compartments is predominantly defined by E_{GSH}. In previous studies, GSH of cardiomyocytes has been quantified by conventional methods including Blue CMAC, mBCl, and HPLC, however, redox couple and compartment-specific measurement of E_{GSH} on either intact cells or even the whole organ has proved difficult (King et al. 2004; Li et al. 2003; Rebrin et al. 2005). The development of fluorescent redox probes expressed as transgenes together with the ability of accurate subcellular localization and high specificity for the redox couple 2GSH/GSSG represent a new tool to fill this gap. At the time of our study, there were Grx1-roGFP2 mouse models for neurons, keratinocytes and erythrocytes as well as Grx1-roGFP2 positive cell lines of HeLa cells and yeast available, but a Grx1-roGFP2 cardiomyocyte-specific mouse line allowing subcellular dynamic analysis of E_{GSH} was lacking (Guzman et al. 2010; Breckwoldt et al. 2014; Wolf et al. 2014; Xu et al. 2011; Gutscher et al. 2008; Hanson et al. 2004; Morgan et al. 2011).

The aim of this project was to study and analyze newly developed cardiomyocyte specific Grx1-roGFP2 mouse models to gain a better insight in E_{GSH} of both the mitochondrial matrix and cytoplasm and to potentially establish a biosensor mouse model for specific and dynamic real-time measurements of E_{GSH}. Therefore, the following aims were formulated for this thesis:

(i) Does the insertion of a Grx1-roGFP2 sensor in the mitochondrial matrix and cytosol lead to cardiac impairment?

(ii) If normal cardiac function is maintained, is both the cytosolic and mitochondrial E_{GSH} of cardiomyocytes within the sensing range of the Grx1-roGFP2 sensor and does it show dynamic, reversible responses as in other biosensor models?

(iii) Do the cytoplasm and mitochondrial matrix differ in their E_{GSH}?

(iv) Can measurements using the Grx1-roGFP2 sensor be performed on both isolated cardiomyocytes and whole hearts *ex vivo*, and do differences emerge in comparison of isolated cardiomyocytes vs. cardiomyocytes in cardiac tissue?

2 Material and Methods

2.1 Material

2.1.1 Chemicals & enzymes

The chemicals and enzymes used in this thesis are listed in **Table 1**.

Table 1: Chemicals and enzymes

Chemical/enzyme	Company
1,4-Dithiothreitol (DTT)	Carl Roth GmbH
2,3-Butanedione monoxime (BDM)	Sigma Aldrich
2.5% Trypsin	Gibco
4-(2-Hydoxyethyl)-1-piperazineethanesulfonic acid (HEPES)	Carl Roth GmbH
Bovine serum albumin (BSA)	AppliChem
Calcium chloride dihydrate ($CaCl_2$ x $2H_2O$)	Sigma Aldrich
Diamide	Sigma Aldrich
Ethylenediaminetetraacetic acid (EDTA)	Carl Roth GmbH
Fluoromount™ aqueous mounting medium	Sigma Aldrich
Glucose	Carl Roth GmbH
Hydrogen Peroxide (H_2O_2)	Carl Roth GmbH
Isoflurane	Abbvie
Laminin	Sigma Aldrich
Liberase DH	Roche
Magnesium chloride ($MgCl_2$)	Carl Roth GmbH
Magnesium sulfate heptahydrate ($MgSO_4$ x 7 H_2O)	Carl Roth GmbH
MitoTracker Deep Red FM	Thermo Fisher Scientific
MyFi™ Mix (Mastermix)	Bioline
Paraformaldehyde (PFA)	Carl Roth GmbH
Phenol Red sodium salt	Sigma Aldrich
Potassium bicarbonate ($KHCO_3$)	Sigma Aldrich
Potassium chloride (KCl)	Carl Roth GmbH
Potassium dihydrogenphosphate (KH_2PO_4)	Carl Roth GmbH
Sodium bicarbonate ($NaHCO_3$)	Carl Roth GmbH
Sodium chloride (NaCl)	Carl Roth GmbH
Sodium dihydrogen phosphate (NaH_2PO_4)	Carl Roth GmbH

Chemical/enzyme	Company
Sodium hydroxide (NaOH)	Carl Roth GmbH
Sodium phosphate dibasic (Na_2HPO_4 x 2 H_2O)	Carl Roth GmbH
Taurine	Sigma Aldrich
Tris hydrochloride (Tris/HCl)	Carl Roth GmbH

2.1.2 Buffers & solutions

The buffers and solutions used in this project are given in **Table 2**.

Table 2: Buffers and solutions

Buffer/solution	Composition
Alkaline lysis buffer	25 mM NaOH 0.2 mM EDTA
BDM solution	500 mM BDM
BSA solution	5 g BSA 50 mL H_2O dest.
Calcium chloride solution 10 mM	10 mL Calcium chloride solution 100mM 90 mL H_2O dest.
Calcium chloride solution 100 mM	1.47 g $CaCl_2$ x $2H_2O$ 100 mL H_2O dest.
Digestion buffer	29.6 mL Perfusion buffer 1x 3.75 µL $CaCl_2$ solution 100 mM 200 µL Trypsin solution 300 – 450 µL Liberase solution
Imaging Buffer	144 mM NaCl 5.4 mM KCl 1 mM $MgCl_2$ 1 mM $CaCl_2$ 10 mM HEPES pH = 7.3
Liberase solution	50 mg Liberase DH 12 mL H_2O injection grade
MitoTracker solution	10 mL Perfusion buffer 1x (recalcificated) 1.5 µL MitoTracker
Neutralization buffer	40 mM Tris/HCl, pH 5.0
Perfusion buffer 10x	1.13 M NaCl

Buffer/solution	Composition
	47 mM KCl 6 mM KH_2PO_4 6 mM Na_2HPO_4 x $2H_2O$ 12 mM $MgSO_4$ x $7H_2O$ 0.32 mM Phenol Red 120 mM $NaHCO_3$ 100 mM $KHCO_3$ 100 mM HEPES 300 mM Taurine H_2O dest.
Perfusion buffer 1x	100 mL Perfusion buffer 10x 20 mL BDM solution 1 g Glucose 880 mL H_2O dest.
Phosphate buffered saline (PBS)	137 mM NaCl 2.7 mM KCl 4.3 mM Na_2HPO_4 x $7H_2O$ 1.4 mM KH_2PO_4 pH = 7.4
Stopping buffer I	2.25 mL Perfusion buffer 1x 250 µL BSA solution 1.25 µL $CaCl_2$ solution 100 mM
Stopping buffer II	9.5 mL Perfusion buffer 1x 500 µL BSA solution 3.75 µL $CaCl_2$ solution 100 mM
Trypsin solution	200 µL Trypsin 2.5% per aliquot
Tyrode solution	128.3 mM NaCl 4.7 mM KCl 1.36 mM $CaCl_2$ 1.05 mM $MgCl_2$ 20.2 mM $NaHCO_3$ 0.42 mM NaH_2PO_4 10 mM Glucose

2.1.3 Software

Table 3 gives an overview of the software used in this project.

Table 3: Software

Software	Application	Reference
Axio Vision	Image acquisition and analysis	Carl Zeiss
GraphPad Prism 4.0	Statistical analysis	GraphPad Software
CorelDraw	Image editor	Corel Corporation
VisiView	Image acquisition and analysis	Visitron Systems GmbH
Windows Office Excel 2013	Data analysis	Windows
InkScape	Image editor	InkScape Community (inkscape.org/de)
Citavi	Bibliographic references	Swiss Academic Software GmbH

2.1.4 Microscope devices

The micrcoscope devices are listed in **Table 4**.

Table 4: Microscope devices

Instrument	Application	Company
Axio Observer D1 microscope	Image acquisition of Grx1-roGFP2 expression	Carl Zeiss
LSM 510 Meta confocal microscope	Image acquisition of mitochondrial fluorescence staining	Carl Zeiss
LCI Plan-Neofluar 63x/1.3na objective	Image acquisition of mitochondrial fluorescence staining	Carl Zeiss
IX 83 inverted microscope	Image acquisition of redox measurements (Isolation)	Olympus
Polychrome V monochromator	Light source	Till Photonics
SMZ1500 Stereomicroscope	Image acquisition of redox measurements on perfused hearts	Nikon Instruments

2.2 Methods

2.2.1 Generation of cardiomyocyte specific Grx1-roGFP2 mice

For studying E_{GSH} in cardiac tissue, a transgenic cardiac myocyte specific mouse model needed to be established. The generation of the αMHC-Grx1-roGFP2 mouse model was done by the Department of Cardiovascular Physiology, Göttingen. The generated transgenic mouse lines express the Grx1-roGFP2 sensor either in the cytosol (Grx1-roGFP2 cyto) or in the mitochondrial matrix (Grx1-roGFP2 mito) of the cardiomyocytes. A vector named pLPCX-Grx1-roGFP2 containing the DNA sequence of the Grx1-roGFP2 sensor with or without a mitochondrial targeting sequence (Neurospora crassa ATP synthase protein 9) (both were kindly provided by Prof. Tobias P. Dick, Heidelberg) was used for the generation. This vector was digested with the restriction enzymes HindIII and XhoI. To achieve a specific expression in cardiomyocytes, an α-myosin heavy chain (αMHC) promoter was applied. Therefore, the vector αMHCpmEpac1 was cut with HindIII and XhoI and Grx1-roGFP2 with or without the mitochondrial targeting sequence were inserted (**Figure 6**). The resulting plasmid was amplified in competent high DH10B Escherichia coli. For preparation and linearization of the DNA an endotoxin-free plasmid kit was used. Subsequently, the DNA was extracted from gels and purified. Generation of transgenic mice was performed via pronuclear injection using C57BL/6N mice (Jackson Laboratories). Transgenesis was done by the core facility of the Max Planck Institute of Experimental Medicine, Goettingen. Seven founder lines for the Grx1-roGFP2 cyto and four founder lines for the Grx1-roGFP2 mito mouse lines tested positive for the expression of the fluorescent sensor protein were generated. For each compartment, two founder mouse lines (mito1, mito2, cyto1 and cyto2) were chosen to be further characterized. Adult male and female animals at the age of 8 to 14 weeks were used for regular experiments. At 60 weeks of age, the oldest animals analyzed for this study showed no signs of premature death, impaired cardiac function, or reduction in Grx-roGFP2 expression. All animal work conformed with institutional guidelines and was approved by the Niedersächsische Landesamt für Verbraucherschutz und Lebensmittelsicherheit (approval number 3392-42502-04-13/1208).

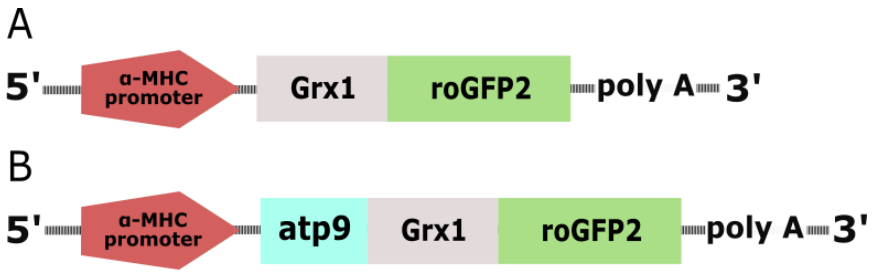

Figure 6: Schematic of the promotor and coding sequence of the plasmids used for generating transgenic biosensor mice. (A) The vector for the generation of redox-sensitive green fluorescent proteins (roGFP2) fused with glutaredoxin-1 (Grx-1) in Grx1-roGFP2 cyto mice were linked to an α-myosin heavy chain (αMHC) promotor sequence to obtain a specific expression in cardiomyocytes. **(B)** In addition to the αMHC promotor sequence, the mitochondrial targeting sequence ATP-synthase protein 9 (atp9) was cloned into the vector for the Grx1-roGFP2 mito mice.

2.2.2 Genotyping Polymerase Chain Reaction (PCR)

The genotyping of the founder mice and their resulting heterozygous offspring was performed with a standard PCR. 75 µL of alkaline lysis buffer was added to the mouse tail biopsies and kept for 1 hour at 95°C followed by 10 min at 4°C to stop the lysis. Subsequently, 75 µL of neutralization buffer was added. The PCR reaction (in total 25 µL) was prepared as follows:

Mastermix	12.5 µL
Primer mroGFP-fwd 5'-CCCTCTCTTTCTCTGCCCAG-3'	0.3 µL
Primer mrogfp-rev 5'-ATAAAGACTCGCGGCACCGT-3'	0.3 µL
DNA template	5 µL
H_2O	6.9 µL

The following parameters were used for the PCR analysis (**Table 5**):

Table 5: roGFP2 PCR reaction

Step	Temperature	Time	Cycles
Initial denaturation	95 ° C	3 mins	1
Denaturation	95 ° C	30 secs	40
Annealing	63 ° C	30 secs	
Elongation	72 ° C	90 secs	
Final Elongation	72 °C	10 mins	1

The resulting PCR products were seperated on an agarose gel. The resulting fragment for Grx1-roGFP2 cyto was 500 bp long, the one for the Grx1-roGFP2 mito 710 bp. Based on the results of genotyping, Grx1-roGFP2 positive were paired with wildtype (wt) animals to generate heterozygous offspring.

2.2.3 Echocardiography

To assess the cardiac heart function of the mice, an echocardiography was performed by Dr. Aline Jatho (Department of Cardiovascular Physiology, Göttingen). The echocardiography and measurement of anterior and posterior wall thickness (AWTh, PWTh), ejection fraction (EF), fractional area shortening (FAS), left ventricular dimension in systole, and left ventricular dimension in diastole were performed according to the protocol described in (Silter et al. 2010). Therefore, mice were anesthetized with 1% isoflurane. Using the parasternal long and short axis view at midpapillary level, two-dimensional images and M-mode tracings were recorded (Vevo 2100 system, Visual Sonics Inc, Toronto, Canada). FAS and EF were used as markers to evaluate the cardiac contractile function.

2.2.4 Preparation and isolation of the transgenic cardiomyocytes and hearts

To determine the E_{GSH} in the cardiac tissue, the hearts had to be removed from the thorax of the mice. Therefore, the mice were anesthetized with isoflurane and killed via cervical dislocation. After the surgical extraction of the heart, depending on whether single cardiomyocytes or whole hearts were required for imaging, the procedure was continued as described below.

The cardiomyocytes of both the Grx1-roGFP2 cyto and Grx1-roGFP2 mito mouse lines were isolated via Langendorff perfusion. The procedure of isolation used in this thesis was based on the protocol described in Börner et al. (2011). The surgically extracted heart was then transferred to an ice-cold PBS containing dish and the aorta was cannulated with a 21G needle. The heart was perfused for 3 min with perfusion buffer 1x followed by 30 mL of digestion buffer, both at a speed of 3.5 mL/min and a temperature of 37°C. Afterwards, the atria were removed and the ventricles were cut into small pieces for 30 sec in 2.5 mL digestion buffer. Stopping buffer I was added to the cell suspension to stop digestion and then the suspension was homogenized for 3 min by using a small needle-free syringe. The isolated cardiomyocytes were filtered through a piece of gauze into a small tube. After 10 min of sedimentation, the supernatant was taken off and the settled cells were resuspended with stopping buffer II. Following this, the concentration of $CaCl_2$ was gradually increased according to **Table 6**. The consecutive steps were performed in intervals of 4 min.

Table 6: Recalcification of isolated cardiomyocytes

Volume of $CaCl_2$ solution	Concentration of $CaCl_2$ solution	Final Ca^{2+} concentration
50 µL	**10 mM**	**62 µM**
50 µL	**10 mM**	**112 µM**
100 µL	**10 mM**	**212 µM**
30 µL	**100 mM**	**500 µM**
50 µL	**100 mM**	**1000 µM**

To culture the isolated cardiomyocytes, coverslips were placed into 6-well-plates and coated with laminin. A drop of 100 µL cell solution was pipetted on each laminin coated coverslip and the plates were incubated at 37°C and 5% CO_2 for at least 1 hr.

For whole heart imaging (WHI), the hearts of mito1 and cyto1 were transferred after surgical extraction to a cold bath of Tyrode solution and the aorta was cannulated with a 21G needle so that the hearts could be retrogradely perfused in a Langendorff mode. The hearts were perfused at a constant pressure with Tyrode solution, which was heated to 37°C and equilibrated with 95% O_2 and 5% CO_2 and were then directly used for further experiments.

2.2.5 Quantification of the expression and localization of the Grx1-roGFP2 sensor

To evaluate the expression of the transgenic sensor in the mouse lines, isolated cardiomyocytes were prepared for a comparative imaging using the bright-field and green fluorescent channels. Cardiomyocyte-containing cover slips were washed with PBS to remove unattached cells before they were mounted on glass slides coated with Mowiol. After drying, cover slips were utilized for imaging with a fluorescence microscope (Axio Observer D1, Zeiss, Germany, Axiovision Software). Bright-field and green fluorescence images were taken for each mouse line and wild type (wt) animals. Matching images were compared and the percentage of Grx1-roGFP2 positive cells was determined.

To identify the co-localization (Grx1-roGFP2 mito) and the non-co-localization (Grx1-roGFP2 cyto) of the Grx1-roGFP2 sensor in the mitochondria, a mitochondrial fluorescence staining and imaging was performed. MitoTracker staining was performed for each of the four mouse lines. Each cardiomyocyte containing coverslip was covered with 500 µL of MitoTracker solution and kept in the incubator for 20 min at 37°C. To fix the staining, cells were treated with PFA 4% for 20 min. The coverslips were mounted onto glass slides using Fluoromount™. In between each step the cells were washed three to four times with PBS. The dried glass slides were then used for imaging.

For imaging, glass slides were analyzed with a confocal laser scanning microscope (LSM 510 Meta confocal laser scanning microscope, Carl Zeiss, Jena, Germany, equipped with a 63x Plan-Neofluoar 1.3NA water-corrected objective). The dyed cardiac myocytes were excited at 488 nm to determine the localization of the Grx1-roGFP2 sensor as well as at 644 nm to identify the dyed mitochondria. The emitted light was detected at 510 nm (Grx1-ro GFP sensor) and 665 nm (MitoTracker). 6 z-series optical sections with steps of 0.05 microns were taken to enable detailed studies and were presented as maximum z-projections. The resulting images of each mouse line were identically adjusted in gamma, brightness, and contrast using Adobe Photoshop CS2.

2.2.6 Redox measurements

Isolated cardiomyocytes prepared as described in section 2.2.4 were used for redox measurements. The incubated coverslips were placed into an imaging chamber at room temperature and washed once with 400 µL of imaging buffer to remove unattached cells followed by another addition of 400 µL of imaging buffer without removing. For imaging, an inverted fluorescent microscope IX38 (Olympus) and Visiview software were used. The Grx1-roGFP2 sensor was excited at 405 nm and 488 nm using a Polychome V light source (Till Photonics). A CCD camera (emission filter 510 ± 10) detected the emitted light. Cardiomyocytes were chosen using live fluorescence light to find cells with optimal sensor expression. To avoid photobleaching, the intensity of the fluorescence light was set as low as possible (to 4%) and switched off right after an appropriate area has been selected. The exposure time was set to 10 ms, which usually led to a good signal-to-noise ratio. During the experiment, pictures were acquired every 5 sec for both the channels and the ratio of the emitted light intensities $I405$ and $I488$ was recorded. Once the ratio maintained a stable baseline, 400 µL of the desired active agents (H_2O_2, diamide or DTT in various concentrations) diluted in imaging buffer were added into the chamber. The experiment was stopped as soon as the response was maintaining a lasting plateau (**Figure 7**).

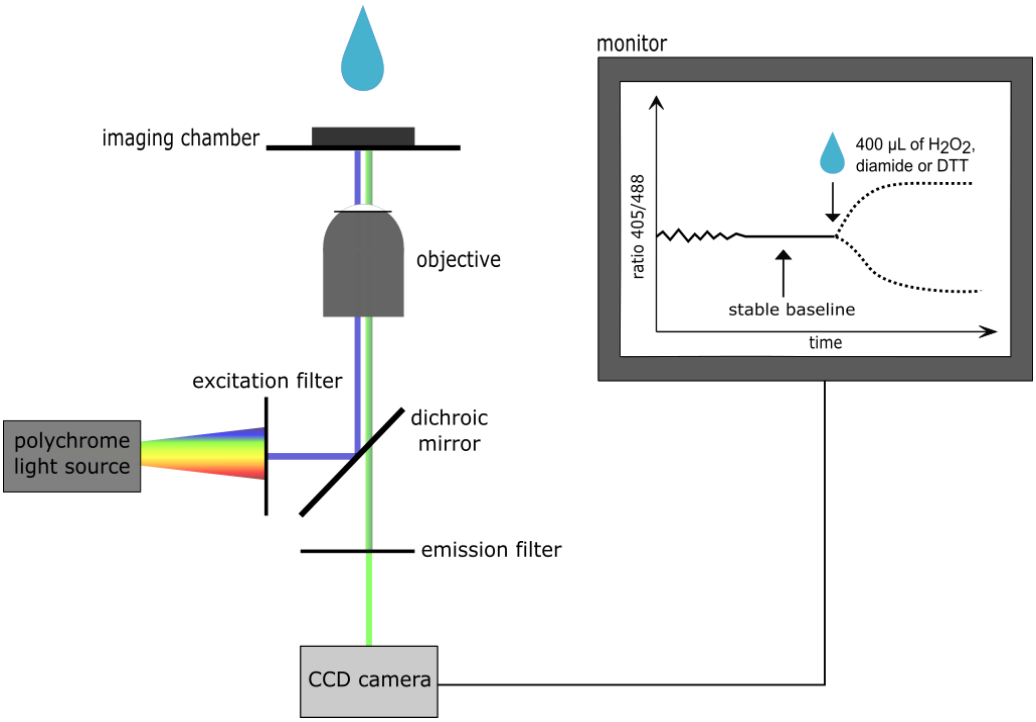

Figure 7: Schematic illustration of the E_{GSH} redox measurements of isolated cardiomyocytes. The isolated cardiomyocytes were excited at 405 and 488 nm and the emitted light was detected via a CCD camera at 510 nm. The ratio 405/488 was observed and by maintaining a stable baseline 400 µL of the desired active agent was added into the imaging chamber. The response to H_2O_2, diamide and DTT were recorded until a lasting plateau was achieved.

For imaging of Langendorff perfused whole hearts a stereo microscope (SMZ1500, Nikon) with 1.5x zoom and a polychrome light source (Till Photonics) controlled by the Visiview Software was used. As for the imaging of isolated cardiomyocytes, the Grx1-roGFP2 sensor was excited at 405 nm and 488 nm and the emitted light detected at 510 nm via a CCD camera (**Figure 8**). Images were acquired every 3 sec with an exposure time of 30 msec. As soon as the 405/488nm ratio reached a stable baseline, the hearts were perfused with the Tyrode solution containing the desired concentration of H_2O_2 or DTT.

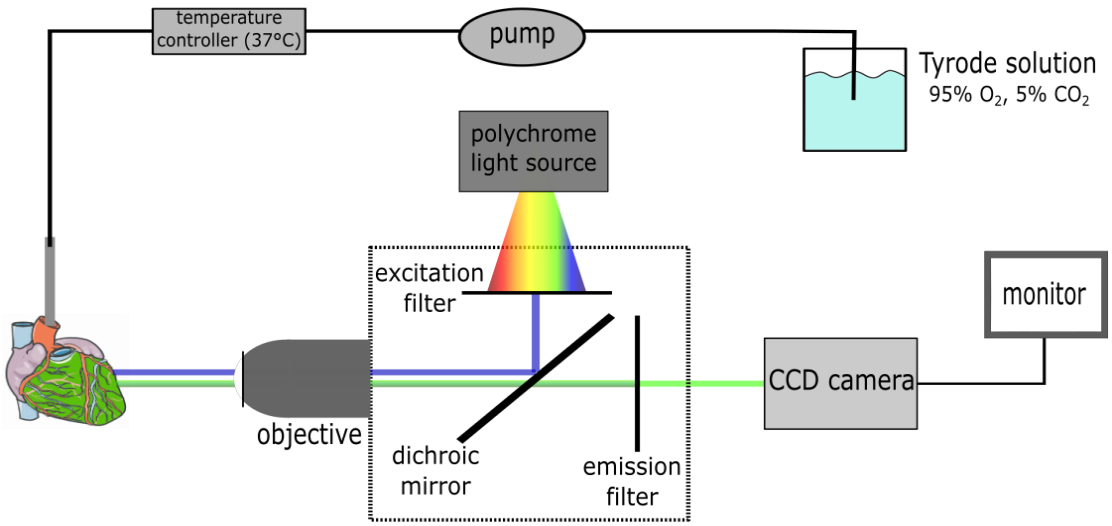

Figure 8: Schematic illustration of Whole Heart Imaging (WHI). Redox measurements were performed using a stereo microscope to image whole hearts perfused with Tyrode solution (95% O2, 5% CO2) containing during the course of the experiments either H2O2 or DTT in different concentrations. After excitation at 405 and 488 nm, the emitted light was detected via a CCD camera and the ratio 405/488 was monitored.

2.2.7 Calculations of the dynamic range and the E_{GSH}

The dynamic range (δ) of a sensor provides information about the possible sensing range which can be obtained via the sensor. δ was determined for each mouse line by dividing the highest ratio in response to H_2O_2 (maximum oxidation) by the lowest ratio in response to DTT (maximum reduction) (Morgan et al. 2011).

The calculations of E_{GSH} in this study are based on the description in Meyer and Dick (2010). Both E_{GSH} and E_{roGFP2} in the cardiac myocytes can be described by the Nernst equation.

$$E_{GSH} = E'^{\circ}_{GSH} - \frac{RT}{2F} \ln\left(\frac{[GSH]^2}{[GSSG]}\right)$$

Equation 1

$$E_{roGFP2} = E'^{\circ}_{roGFP2} - \frac{RT}{2F} \ln\left(\frac{[roGFP2_{red}]}{[roGFP2_{ox}]}\right)$$

Equation 2

R is the gas constant ($8.315 \frac{kgm^2}{s^2 molK}$), T the absolute temperature (310.15 K), and F the Faraday constant ($96\,485 \frac{C}{mol}$). E'°_{GSH} and E'°_{roGFP2} are the midpoint redox potentials under standard conditions ($T = 298.15$ K, $pH = 7.0$), which were determined to be -240 mV and -280 mV, respectively (Dooley et al. 2004; Schafer and Buettner 2001). The potential

difference ΔE acting as the driving force for the exchange of electrons between the two redox couples is characterized by the difference of E_{roGFP2} and E_{GSH}:

$$\Delta E = E_{roGFP2} - E_{GSH}$$

Equation 3

The Grx1-roGFP2 sensor is primarily interacting with the 2GSH/GSSG redox couple. Therefore, an equilibrium between the redox couple of GSH and our Grx1-roGFP2 sensor can be assumed. At equilibrium, $\Delta E = 0$, which means that E_{GSH} is equivalent to E_{roGFP2}. As a result, Equation 3 is converted to the following equation by inserting Equation 1 and Equation 2:

$$E_{\mathrm{GSH}} = E_{\mathrm{roGFP2}}$$

$$\Rightarrow E'^{\circ}_{\mathrm{GSH}} - \frac{RT}{2F}\ln\left(\frac{[GSH]^2}{[GSSG]}\right) = E'^{\circ}_{\mathrm{roGFP2}} - \frac{RT}{2F}\ln\left(\frac{[roGFP2_{\mathrm{red}}]}{[roGFP2_{\mathrm{ox}}]}\right)$$

Equation 4

As we are not able to measure exactly $\frac{[GSH]^2}{[GSSG]}$ or $\frac{[roGFP2_{\mathrm{red}}]}{[roGFP2_{\mathrm{ox}}]}$, we used the degree of oxidation (OxD), which represents the fraction of the oxidized form of the total intracellular amount of Grx1-roGFP2 and GSH.

$$OxD_{\mathrm{GSH}} = \frac{2[GSSG]}{[GSH] + 2[GSSG]} = \frac{2[GSSG]}{GSH_{\mathrm{total}}}$$

Equation 5

$$OxD_{\mathrm{roGFP2}} = \frac{[roGFP2_{\mathrm{ox}}]}{[roGFP2_{\mathrm{ox}}] + [roGFP2_{\mathrm{red}}]}$$

Equation 6

After transposing Equation 5 and Equation 6, they can be transferred to Equation 4.

$$E_{\mathrm{GSH}} = E'^{\circ}_{\mathrm{GSH}} - \frac{\mathrm{RT}}{2\mathrm{F}}\ln\left(\frac{2GSH_{\mathrm{total}}(1 - OxD_{\mathrm{GSH}})^2}{OxD_{\mathrm{GSH}}}\right)$$
$$= E'^{\circ}_{roGFP2} - \frac{\mathrm{RT}}{2\mathrm{F}}\ln\left(\frac{1 - OxD_{\mathrm{roGFP2}}}{OxD_{\mathrm{roGFP2}}}\right) = E_{\mathrm{roGFP2}}$$

Equation 7

This shows that the $\mathrm{OxD}_{\mathrm{roGFP2}}$ needs to be defined to determine E_{GSH}. Assuming that in every cardiomyocyte each oxidized roGFP2 molecule emits its own light after excitation at 405 nm, the measured intensity $I405$ represents the total amount of these emissions. $I488$ is correspondingly characterized by the reduced roGFP2 molecules. These two measured variables are related by defining the fluorescence ratio $r = \frac{I405}{I488}$. As r describes the redox state under resting conditions, $r_{\mathrm{ox}} = \frac{I405_{\mathrm{ox}}}{I488_{\mathrm{ox}}}$ and $r_{\mathrm{red}} = \frac{I405_{\mathrm{red}}}{I488_{\mathrm{red}}}$ display the state upon

maximum oxidation and reduction. Accordingly, $I405_{ox}$, $I488_{ox}$, $I405_{red}$, and $I488_{red}$ are the intensities emitted at the state of full oxidation and reduction, respectively. OxD_{roGFP2} is defined as the amount of oxidized roGFP2 among the total amount of roGFP2 (see Equation 6). The total roGFP2 molecules contributing either to $I405$ or $I488$ depending on their redox form are reflecting the current redox state of the total roGFP2 and thus, OxD_{roGFP2} as well. Considering both the limiting conditions upon maximum oxidation and reduction and the measurement under resting conditions, OxD_{roGFP2} can be described using the measured fluorescence intensities:

$$\boldsymbol{OxD_{roGFP2}} = \frac{\frac{\boldsymbol{I405}}{\boldsymbol{I488}} - \frac{\boldsymbol{I405_{red}}}{\boldsymbol{I488_{red}}}}{\frac{\boldsymbol{I488_{ox}}}{\boldsymbol{I488_{red}}}\left(\frac{\boldsymbol{I405_{ox}}}{\boldsymbol{I488_{ox}}} - \frac{\boldsymbol{I405}}{\boldsymbol{I488}}\right) + \left(\frac{\boldsymbol{I405}}{\boldsymbol{I488}} - \frac{\boldsymbol{I405_{red}}}{\boldsymbol{I488_{red}}}\right)}$$

Equation 8

To investigate OxD_{roGFP2} and accordingly E_{GSH}, the Grx1-roGFP2 sensor needs to be set both in a fully oxidized and reduced state. The isolated cardiomyocytes can either be maximally reduced or oxidized in the following experiments, so that E_{GSH} is not calculated for each cell itself. Instead, the mean glutathione redox potential $\bar{E}_{GSH}$ was determined for each mouse line. Therefore, the baseline intensities of each cell were normalized ($r = \frac{I405}{I488} = 1$) and the mean fluorescence intensities $\overline{I405}_{ox}$, $\overline{I488}_{ox}$, $\overline{I405}_{red}$, and $\overline{I488}_{red}$ were calculated for corresponding cells of each mouse line. These values were inserted into Equation 8 and the resulting OxD_{roGFP2} was used to determine $\bar{E}_{GSH}$ with Equation 7.

Though the measured ratio of the Grx1-roGFP2 sensor is not affected by pH changes (Gutscher et al. 2008; Schwarzländer et al. 2008), the redox potential of both GSH and roGFP2 is influenced by the pH due to the protons involved in the disulfide bond building process. The change of the midpoint redox potential $E^{\circ\prime}_{roGFP2}$ according to pH changes is described in Cannon and Remington 2008:

$$\boldsymbol{E^{\circ\prime}_{pH}} = \boldsymbol{E^{\circ\prime}_{roGFP2}} - \mathbf{0.198\ T} * (\mathbf{pH} - \mathbf{7})$$

Equation 9

T is the absolute temperature and pH describes the pH of the cell compartment in which the sensor is localized.

The redox potentials were calculated with mean values of $\overline{I405}_{ox}$, $\overline{I488}_{ox}$, $\overline{I405}_{red}$, and $\overline{I488}_{red}$ derived from multiple redox measurements, which means, that the standard deviation (SD) and standard error of the mean (SEM) need to be considered. These SEM are propagated to the determination of the redox potentials as it has been calculated with Equation 8 and Equation 7 using these mean values. The error of OxD_{roGFP2} (ΔOxD) and E_{GSH} (ΔE_{GSH}) were determined as follows:

$$\Delta \boldsymbol{OxD} = \sqrt{\left(\frac{\boldsymbol{dOxD}}{\boldsymbol{dI405_{ox}}} * \Delta \boldsymbol{I405_{ox}}\right)^2 + \left(\frac{\boldsymbol{dOxD}}{\boldsymbol{dI488_{ox}}} * \Delta \boldsymbol{I488_{ox}}\right)^2 + \left(\frac{\boldsymbol{dOxD}}{\boldsymbol{dI405_{red}}} * \Delta \boldsymbol{I405_{red}}\right)^2 + \left(\frac{\boldsymbol{dOxD}}{\boldsymbol{dI488_{red}}} * \Delta \boldsymbol{I488_{red}}\right)^2}$$

Equation 10

$$\Delta \boldsymbol{E_{GSH}} = \frac{\mathbf{RT}}{\mathbf{2F}\left(OxD_{\mathrm{roGFP2}} - OxD_{\mathrm{roGFP2}}{}^2\right)} * \Delta \boldsymbol{OxD}$$

Equation 11

Both the equations are based on the Gaussian error propagation. $\frac{dOxD}{dI}$ is the differentiation of Equation 8 with respect to the fluorescence intensity as indicated.

2.2.8 Statistics

For analyzing the data of the measurements with the Grx1-roGFP2 sensor, the intensity profile of both the 408 nm and 488 nm channels were exported to Microsoft Office Excel 2013. The baseline for both the channels of each measured cell was normalized to 1 and $\boldsymbol{r_{ox}}$ or $\boldsymbol{r_{red}}$ was calculated for the normalized intensities. Maximum responses were sorted by reactive substances added. Redox potential calculations were based on n-number of cardiomyocytes from a-number of independent isolations or mice as indicated in the figure legends. Data is shown as mean ± SEM. Student's two tailed t-test was used to calculate statistical significance between two conditions. By comparison of more than two groups one-way ANOVA (Bonferroni post-hoc test) was performed. The statistical significance was set to $p < 0.05$ (indicated as: *). Statistical analyses were performed using the GraphPad Prism 4 software.

3 Results

3.1 The Grx-roGFP2 sensor is strongly expressed in both Grx1-roGFP cyto and Grx-roGFP2 mito mouse lines

To quantify the abundance of the Grx1-roGFP2 sensor in our Grx-roGFP2 cyto mouse lines cyto1 and cyto2 and the Grx1-roGFP 2 mito mouse lines mito1 and mito2, a comparison of bright field to green fluorescence images were performed for transgenic and wt mice. Wt mice were used to exclude effects of auto-fluorescence, which could influence the quantification of roGFP2 positive cardiomyocytes in the transgenic mouse lines. A positive fluorescence signal upon excitation with 405 nm was assessed as a positive expression of the Grx1-roGFP2 sensor. By merging bright field with fluorescence images, roGFP2 positive cells could be distinguished from non-positive cells. Whereas the transgenic mouse lines showed a clear signal of the Grx1-roGFP2 sensor, the wt mice remained without any fluorescence signal. The Grx1-roGFP2 mito mouse lines showed a minimally higher number of roGFP2 positive cells than the Grx1-roGFP2 cyto mouse lines (**Figure 9**). The percentage of Grx1-roGFP2 positive cardiac myocytes was determined from different isolations for each transgenic mouse line and showed an unequivocal expression of Grx1-roGFP2 in cardiac myocytes (**Figure 10**).

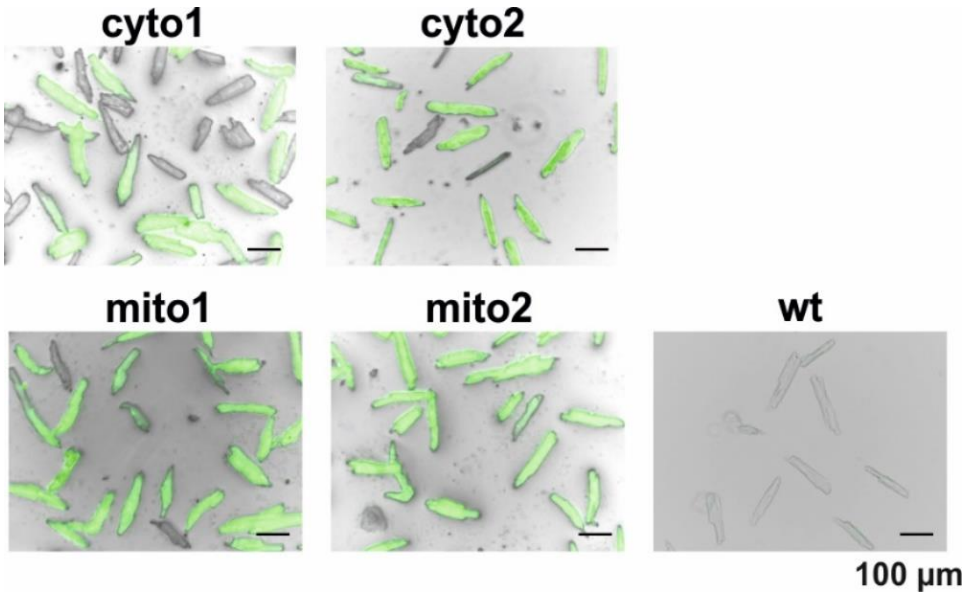

Figure 9: Clear expression of the Grx1-roGFP2 biosensor in both cyto and mito mouse lines compared to wt mice. The cardiomyocytes from cyto1, cyto2, mito1, mito2 and wild type (wt) mice were isolated via Langendorff perfusion and incubated at 37°C and 5% CO_2. The fluorescence images of cardiomyocytes exposed to 405 nm were overlaid with bright field images to identify roGFP2 positive cells.

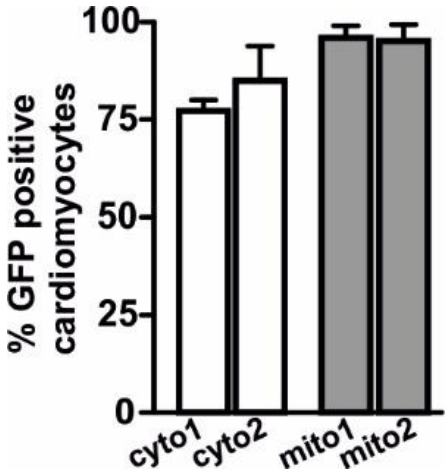

Figure 10: Quantification of roGFP expressing cardiomyocytes in Grx1-roGFP2 cyto and mito mouse lines. Grx1-roGFP2 positive cells were quantified by comparing bright-field to fluorescence images. For each indicated mouse line values of isolations of 3 independent mice were included and > 50 cardiomyocytes per mouse were quantified. Mean ± SEM.

3.2 The Grx1-roGFP2 sensor in the Grx1-roGFP2 mito mouse lines is localized to the mitochondria whereas no co-localization in Grx1-roGFP2 cyto mice is observed

The Grx1-roGFP2 sensor was targeted either to the mitochondrial matrix of the cardiomyocytes or non-targeted (cyto). In order to verify the correct localization of the sensor, isolated cardiomyocytes of all analyzed mouse lines were stained with red MitoTracker solution. Deep Red MitoTracker was chosen to avoid possible interference between the excitation and emission of the Grx1-roGFP2 sensor. The emission of the sensor was detected at 510 nm, the one of the MitoTracker at 665 nm. Mito1 and mito2 cardiomyocytes showed a significant signal of both the Grx1-roGFP2 sensor (green) and the MitoTracker (red). Merged together, the signals appeared universally colocalized, meaning that the sensor in these mouse lines is localized to the mitochondria. Likewise, significant signals were detected for both cyto1 and cyto2. In the overlay, however, no colocalization could be detected. This shows that the sensor of the cyto mouse lines is not localized to the mitochondria but to the surrounding cytoplasm. For wt cardiomyocytes no signal of the Grx1-roGFP2 sensor was detectable, whereas the signal of the MitoTracker was again significant (**Figure 11**). Based on these results, we were able to verify the correct localization of our sensor in the analyzed mouse lines.

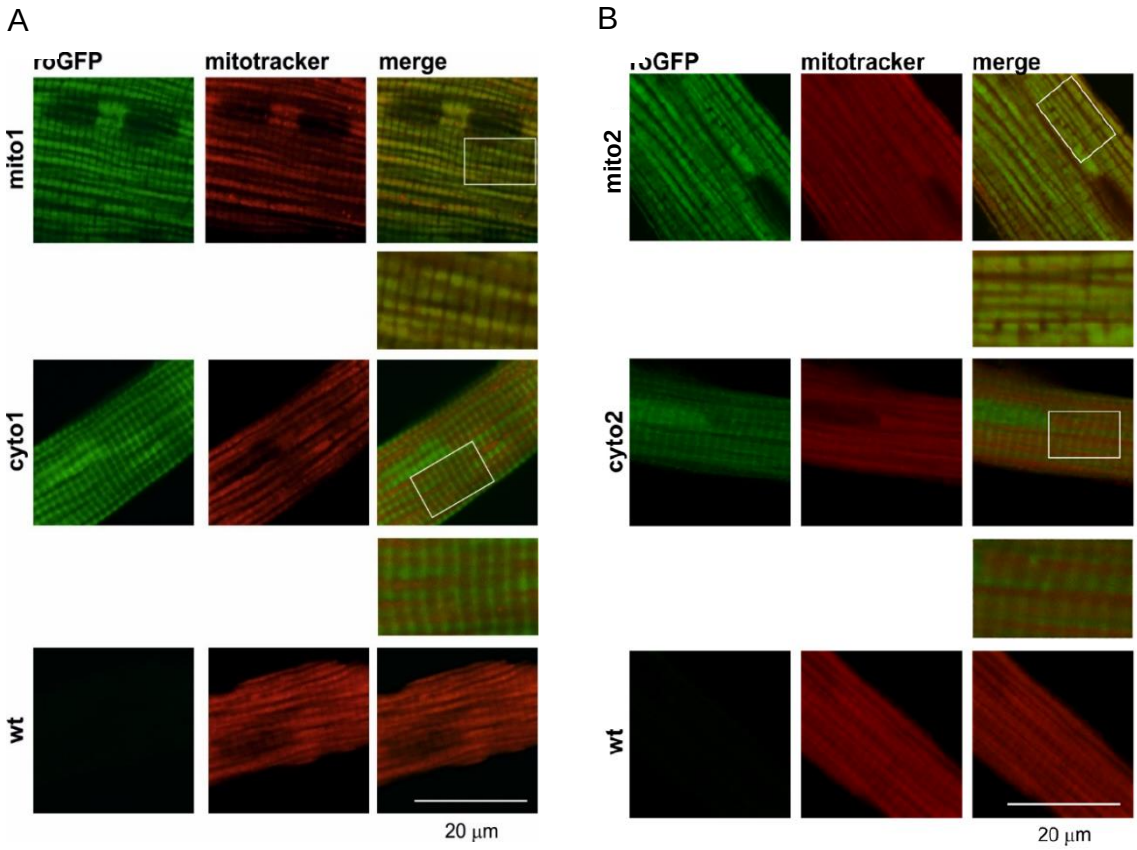

Figure 11: Colocalization of DeepRed MitoTracker and Grx1-roGFP2 in both mito mouse lines, but not in the cyto mouse lines. Isolated cardiomyocytes of mito1, cyto1 **(A)**, mito2, cyto2 **(B)**, and wild type (wt) mice were exposed to both 488 nm and 644 nm. Images of the fluorescence signals at 510 nm (green) and 665 nm (red), respectively, were taken and merged to prove, whether there was a colocalization of the DeepRed Mito Tracker and the Grx1-roGFP2 biosensor.

3.3 Transgenic expression of Grx1-roGFP2 in cardiac myocytes does not affect heart function

Echocardiography was performed to exclude any detrimental influence on the mouse hearts due to the transgenic expression of the biosensor. To analyze the heart function, AWTh, PWTh, EF and FAS of the transgenic mouse lines were measured in comparison to corresponding wt littermates as described in chapter 2.2.3. Both AWTh and PWTh as well as EF and FAS of the transgenic hearts showed no significant deviation of the cardiac function (**Figure 12**). Hence, we were able to exclude cardiotoxic effects of the Grx1-roGFP2 sensor on the hearts.

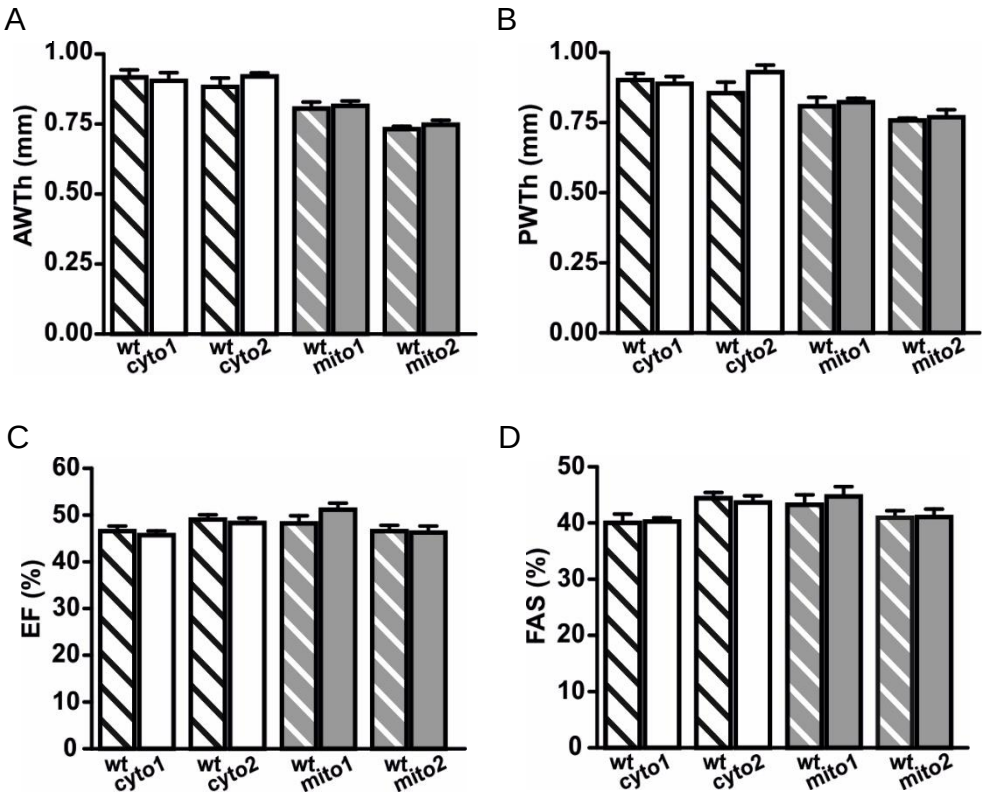

Figure 12: Echocardiography of transgenic and corresponding wt mice. Echocardiography was performed with 4 to 7 mice per genotype and corresponding wild type (wt). **(A)** Anterior wall thickness (AWTh), **(B)** posterior wall thickness (PWTh), **(C)** ejection fraction (EF), **(D)** fraction area shortening (FAS). Data are presented as mean ± SEM.

3.4 The Grx1-roGFP2 sensor showed a dynamic response to H_2O_2 and DTT

The protonation state of the cysteine residues of the roGFP2 affects its fluorescence. Oxidizing conditions lead to a disulfide bond conformation, which in turn shifts the excitation maximum near 405 nm, whereas a reducing environment leads to an excitation maximum near 488 nm. In both cases, the emission is detected at 510 nm. The fusion of the Grx1 to the roGFP2 catalyzes specifically the reaction between roGFP2 and GSH. First, we wanted to prove, whether the Grx1-roGFP2 sensor localized to cardiomyocytes reacts to changes of E_{GSH}. Isolated Grx1-roGFP2 positive cardiomyocytes of mito1, mito2, cyto1 and cyto2 mice were isolated and measured as described in chapter 2.2.4. To induce redox changes, a bolus of 100 µM H_2O_2 was used as an oxidizing agent whereas 1 mM DTT was used for reduction. The fluorescence ratio 405/488 nm of the cardiomyocytes from each mouse line changed equally according to the applied stimulus: after stimulation with H_2O_2 the excitation maximum was shifted near to 405 nm, leading to an increase of the ratio 405/488 nm. Reducing conditions shifted the excitation maximum near 488 nm, which in turn led to the decrease of the ratio 405/ 488 nm. **Figure 13 A, B** shows an exemplary response of an isolated cardiomyocyte of mito1. The shift of the excitation peak becomes visible by turning from the fluorescence color turquoise to green upon addition of H_2O_2 and to blue upon addition of DTT **(Figure 13 C, D**). Both stimuli lead to a rapid change and stable plateau within <100-200 sec in both mito and cyto mouse lines, which indicates that the Grx1-roGFP2 sensor indeed dynamically reports changes of the redox state in real-time. The change of the fluorescence intensities due to oxidizing or reducing stimuli in each mouse line demonstrates, that the basal mitochondrial and cytosolic E_{GSH} of the cardiomyocytes lie within the effective range of the Grx1-roGFP2 sensor.

Subsequently, single cardiomyocytes of cyto1 and mito1 mice were treated consecutively with H_2O_2 and DTT to demonstrate the reversibility of the disulfide bond formation of the Grx1-roGFP2 sensor (**Figure 14).** After applying a bolus of 100 µM H_2O_2, the cells were washed and then treated with 1 mM DTT. Both the oxidation and reduction of the sensor were comparable to the responses by treatment with only one agent. Therefore, we concluded that the redox reaction is independent of the experimental setting. Due to a higher rate of cell death with the subsequent addition of H_2O_2 and DTT, single bolus treatment was preferred in the following experiments.

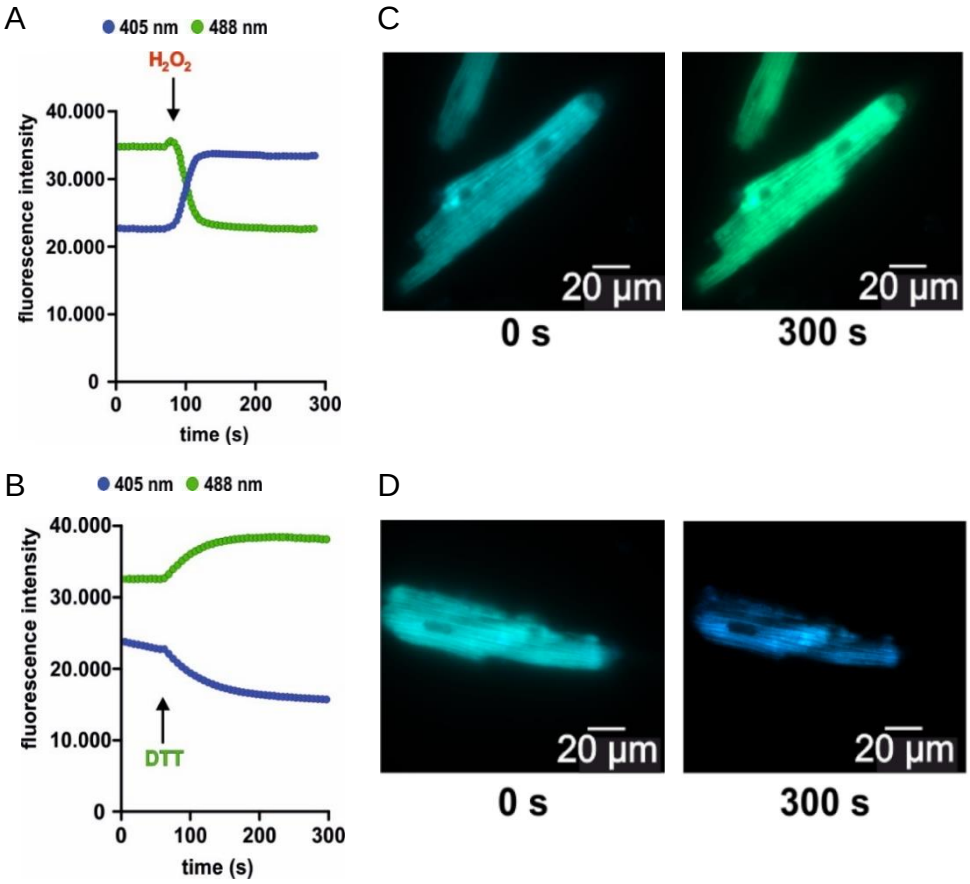

Figure 13: Exemplary response of an Grx1-roGFP2 mito1 cardiomyocyte to 100 µM H_2O_2 and 1 mM DTT. Cardiomyocytes of Grx1-roGFP2 were isolated and incubated at 37°C and 5% CO2 for 1 hr. The fluorescence intensities of excitations at 405 nm and 488 nm were recorded both before and after the addition of 100 µm H_2O_2 **(A)** and 1 mM DTT **(B)**. In parallel, fluorescence images were taken during the experiments with 100 µM H_2O_2 **(C)** and 1 mM DTT **(D)**. After 300 s the maximum oxidation and reduction was achieved and the visible emission of the cells turned from turquoise to green and blue, respectively.

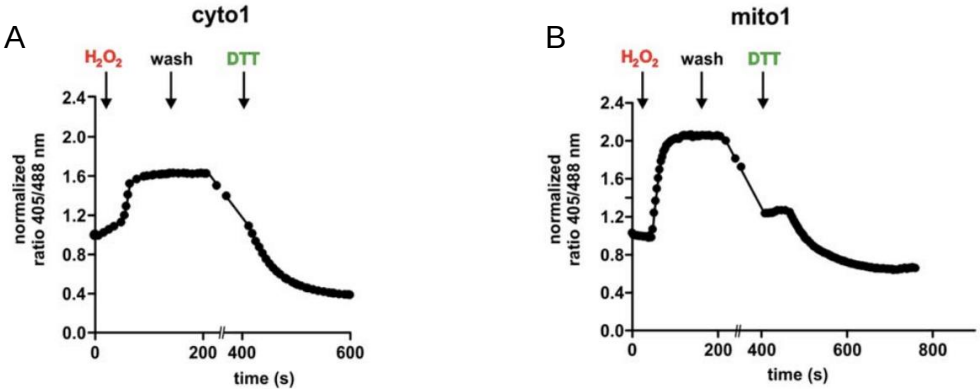

Figure 14: Exemplary Responses of an Grx1-roGFP2 positive cyto1 and mito1 cardiomyocyte to subsequent stimulation with H_2O_2 and DTT. Both the cyto1 **(A)** and mito1 **(B)** cardiomyocyte were first stimulated with 100 µM H_2O_2. After maintaining a stable plateau, the cells were washed and subsequently, 1 mM DTT was added. Ratio of the fluorescence excitation ratio 405/488 nm were recorded.

3.5 Comparison of the E_{GSH} in the cytosol versus mitochondrial matrix

3.5.1 Grx1-roGFP2 cyto and Grx1-roGFP2 mito cardiomyocytes show different maximum oxidative and reductive responses

The Grx1-roGFP2 sensor allows a real-time quantification of the GSH redox pair. Due to its subcellular compartment localization, we were able to define compartment specific E_{GSH}. To gain insight into the redox state of the GSH couple in more detail, we needed to define the concentrations of H_2O_2 and DTT to reach the maximum reduction and oxidation (see 2.2.7). Therefore, different concentrations ranging from 1 to 500 µM of H_2O_2 and 0.02 to 3 mM of DTT were applied to isolated cardiomyocytes of mito1 and cyto1. The maximum responses to these stimuli were recorded until they reached a stable plateau. Finally, we determined the concentrations that are sufficient to generate the maximum sensor oxidation and reduction.

In mito1 and cyto1, maximum oxidizing sensor response is achieved at concentrations ≥ 100 µM H_2O_2 as well as concentrations ≥ 1mM of DTT are sufficient to lead to the maximum reduction (**Figure 15 A,B, Figure 16 A,B**). Subsequently, we verified whether these concentrations of H_2O_2 and DTT were also sufficient to achieve a maximum response in isolated cardiomyocytes of mito2 and cyto2. The addition of 100 µM and 500 µM H_2O_2 both led to an oxidative response without any significant difference between the extent of these responses. Likewise, no significant deviation was observed between the extent of the reductive responses after the addition of 1 mM and 2mM DTT. Thus, maximum sensor responses are also achieved in mito2 and cyto2 at concentrations ≥ 100 µM H_2O_2 and concentrations ≥ 1mM of DTT (**Figure 17**). However, there was a significant difference in the extent of the maximum responses between cyto and mito cardiomyocytes concerning oxidative or reductive stimuli. The mito mouse lines showed a higher increase of the fluorescence ratio after oxidative stimuli compared to the cyto mouse lines, whereas the latter had a stronger decrease of the ratio after addition of DTT. Since these responses differ from the amount of oxidation and reduction, we assumed that there are distinct basal E_{GSH} in the cytosol and the mitochondrial matrix.

Based on the maximum responses to H_2O_2 and DTT of the sensor, the dynamic range δ, that provides information about the sensitivity of the sensor, could be determined for each mouse line. The individual values are shown in **Table 7**. Values from 4.2 to 5.0 were obtained, which corresponds to values in other settings reported in the literature (Morgan et al. 2011).

Since H_2O_2 does not directly interact with the Grx1-roGFP2 sensor but with the endogenous GSH redox pool, additional experiments with diamide were performed with isolated cardiomyocytes. The function of diamide is independent of the cellular GSH pool, as it is a sulfhydryl reagent that directly oxidizes the two thiol groups of the biosensor to a disulfide

bond. The concentrations used were identical to those of H_2O_2, varying from 1 to 500 µM. Comparing the maximum responses of H_2O_2 versus diamide, we could exclude a significant difference between these two oxidizing stimuli (**Figure 15 C**, **Figure 16 C**). This observation demonstrated that the maximum oxidation of the biosensor by H_2O_2 was not limited by the endogenous GSH pool and represented the absolute maximum oxidation. Therefore, the concentration of H_2O_2 used was indeed sufficient to maximally oxidize the Grx1-roGFP2 sensor.

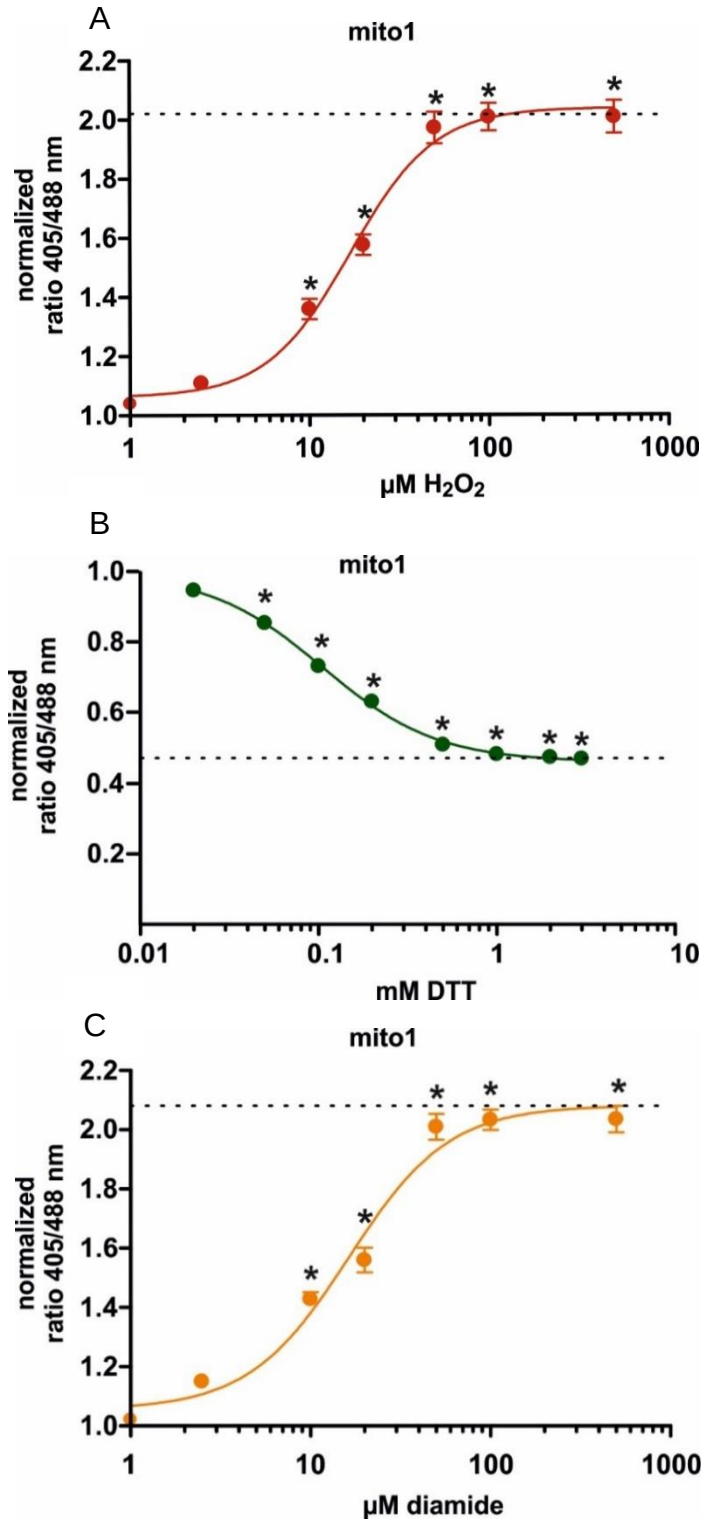

Figure 15: Grx1-roGFP2 response of mito1 to different concentrations of H_2O_2, diamide and DTT. H_2O_2 (1 to 500 µM) **(A)**, diamide (1 to 500 µM) **(B)** and DTT (0.02 to 3 mM) **(C)** were applied to isolated Grx1-roGFP2 mito1 cardiomyocytes. Ratios of the fluorescence excitation at 405/488 nm were recorded. Measurements of isolated cardiomyocytes from 15 (H_2O_2), 11 (diamide) and 17 (DTT) mice were included. Mean ± SEM. *$p < 0.05$ (compared to non-treated control), one-way ANOVA-analysis (Bonferroni post-hoc test).

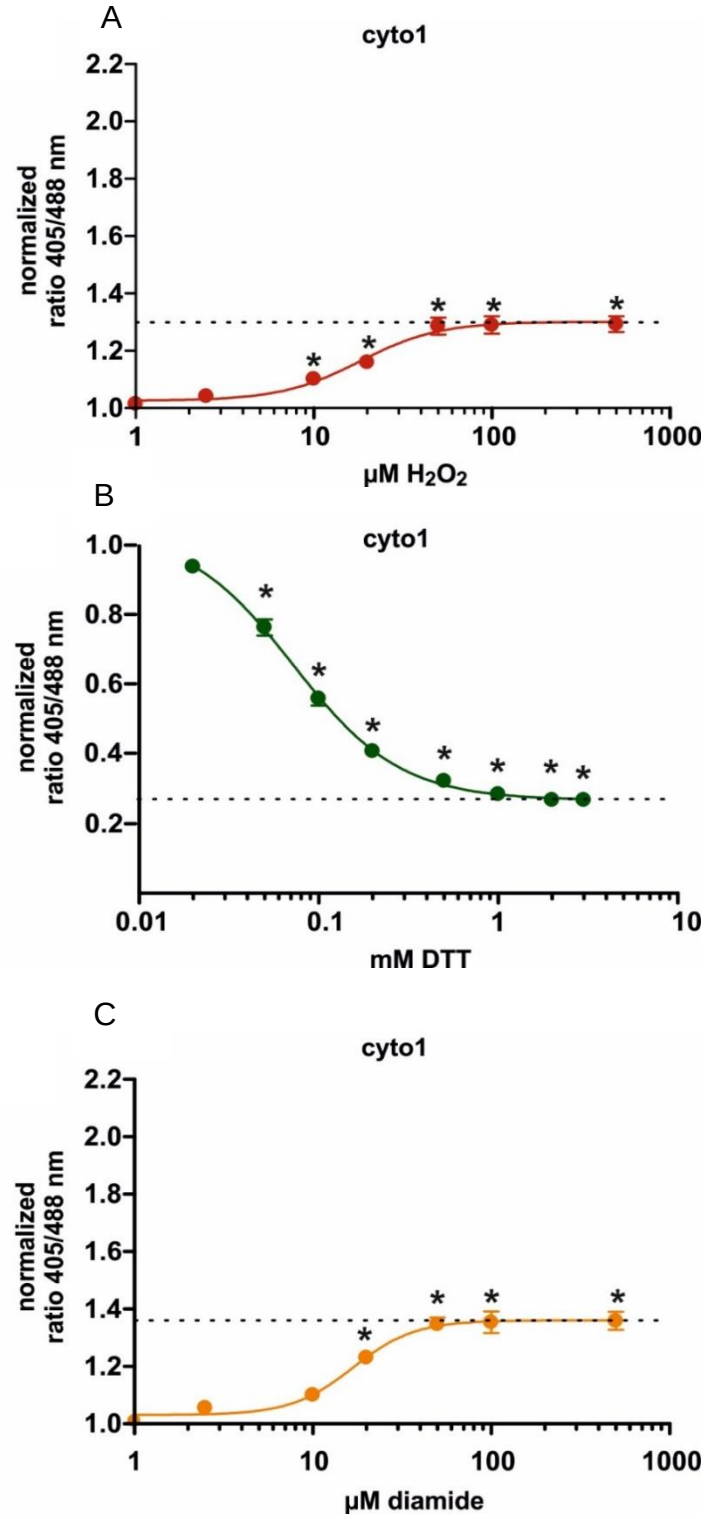

Figure 16: Grx1-roGFP2 response of cyto1 to different concentrations of H_2O_2, diamide and DTT. H_2O_2 (1 to 500 µM) **(A)**, diamide (1 to 500 µM) **(B)** and DTT (0.02 to 3 mM) **(C)** were applied to isolated Grx1-roGFP2 cyto1 cardiomyocytes. Ratios of the fluorescence excitation at 405/488 nm were recorded. Measurements of isolated cardiomyocytes from 18 (H_2O_2), 13 (diamide) and 15 (DTT) mice were included. Mean ± SEM. *$p < 0.05$ (compared to non-treated control), one-way ANOVA-analysis (Bonferroni post-hoc test).

Table 7: Dynamic range (δ) of the Grx1-roGFP2 sensor protein localized to different compartments in isolated cardiomyocytes

	mito1	mito2	cyto1	cyto2
dynamic range δ H_2O_2 – DTT	4.3	4.2	5.0	4.8

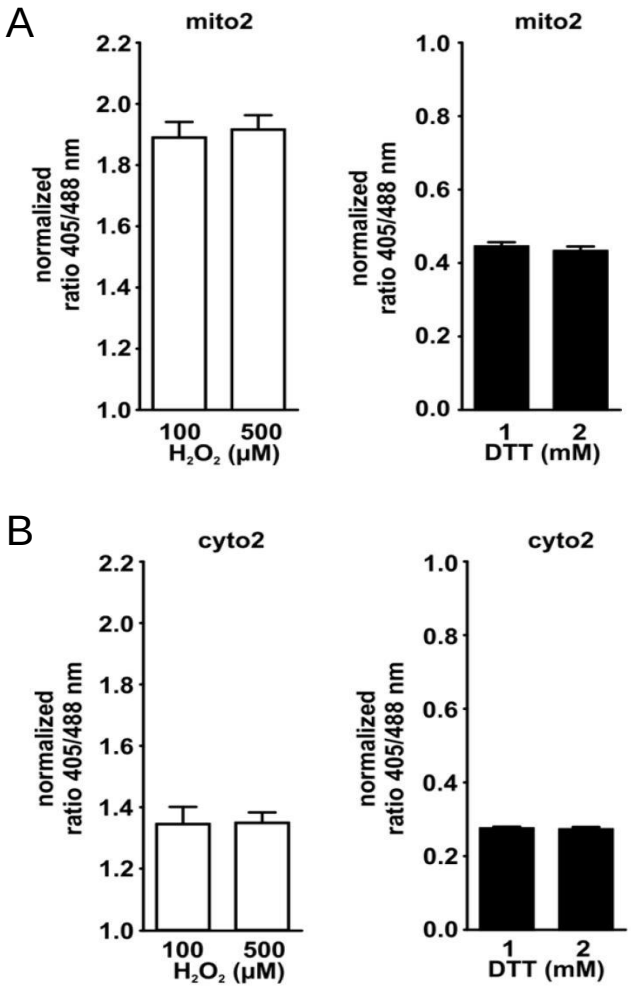

Figure 17: Grx1-roGFP2 response of mito2 and cyto2 to H_2O_2 and DTT. H_2O_2 (100 and 500 µM) and DTT (1 and 2 mM) were applied to isolated Grx1-roGFP2 mito2 **(A)** and cyto2 **(B)** cardiomyocytes. Maximum sensor oxidation and reduction is achieved at 100 µM of H_2O_2 and 1 mM of DTT. Ratios of the fluorescence excitation at 405/488 nm were recorded. For each concentration at least 45 isolated cardiomyocytes from four (mito2) and three (cyto2) mice were included. Mean ± SEM.

3.5.2 The E_{GSH} of the cytosol is less reductive than the E_{GSH} of the mitochondrial matrix

The titration experiments revealed that the cytosol and the mitochondria differ in the extent of their reaction to oxidizing and reducing stimuli. To further define this reaction, the basal E_{GSH} was determined for each mouse line. As described in section 2.2.7, the maximum reduction and oxidation responses were used to calculate the redox potential of both H_2O_2 versus DTT and diamide versus DTT. A comparison of the individual compartments within the respective mouse lines and concerning the use of H_2O_2 and diamide showed that the calculated E_{GSH} yielded comparable values without significant differences. However, the comparison of the $E_{GSH}$of the cytosol and mitochondrial matrix was significant in that the cytosol has a less reducing E_{GSH} than the mitochondrial matrix.

The Grx1-roGFP2 biosensor itself is not pH-dependent, but changes in the pH, which represents the number of free H^+ ions, influence the mid-point redox potential of the 2GSH/GSSG redox couple on which our calculations are based. We therefore took into account in our calculations of the E_{GSH} that the pH in the individual compartments is not equal but 7.4 in the cytosol and 7.91 in the mitochondrial matrix (Llopis et al. 1998). The pH corrected calculations of E_{GSH} also show that the cytosol has a more oxidizing environment than mitochondrial matrix (**Table 8**).

3.5.3 Lack of Ca^{2+} and glucose as well as overnight culturing does not affect the E_{GSH}

In order to exclude any influence of the process of isolation of the cardiomyocytes or the up to here used experimental setting, additional experiments were performed with modified conditions. Since imaging was performed with freshly isolated cardiomyocytes, experiments were repeated with isolated cells cultured over night to exclude effects on the redox potential due to the process of cell isolation and cultivation. Furthermore, to exclude any effects on the E_{GSH} due to starving of the cells or their contractility according to the presence of Ca^{2+}, additional experiments were performed with buffer containing 10 mM of glucose and Ca^{2+} -free imaging buffer. Compared to the regular experimental set-up, experiments with overnight cultured cells, lack of calcium or glucose addition showed no significant difference of the E_{GSH} compared to the experiments demonstrated above (**Table 8**).

Table 8: Calculation of E_{GSH} based on the redox measurements with isolated cardiomyocytes of both the Grx1-roGFP2 mito and cyto mouse lines.

	Mouse line			
E_{GSH}	**mito1**	**mito2**	**cyto1**	**cyto2**
H_2O_2 – DTT	-278.9 ± 0.4 mV (104)	-275.4 ± 0.4 mV (98)	-254.8 ± 0.8* mV (112)	-256.3 ± 0.7* mV (154)
diamide – DTT	-278.9 ± 0.4 mV (108)	-277.1 ± 0.4 mV (97)	-257.2 ± 0.7* mV (102)	-255.8 ± 0.6* mV (154)
H_2O_2 – DTT ph corrected	-333.6 ± 0.4 mV (pH 7.91)	-330.1 ± 0.4 mV (pH 7.91)	-278.8 ± 0.7 mV (pH 7.4)	-280.3 ± 0.7 mV (pH 7.4)
diamide – DTT ph corrected	-333.6 ± 0.4 mV (pH 7.91)	-331.8 ± 0.4 mV (pH 7.91)	-281.2 ± 0.7 mV (pH 7.4)	-279.8 ± 0.7 mV (pH 7.4)
Ca^{2+}-free buffer	-274.2 ± 0.8 mV (30)	-274.8 ± 0.7 mV (28)	-254.8 ± 1 mV (102)	-255.5 ± 0.8 mV (102)
+10 mM glucose	-273.1 ± 1 mV (18)	-276.9 ± 0.9 mV (35)	-258.5 ± 0.8 mV (27)	-255.5 ± 0.9 mV (25)
overnight culture	-277.4 ± 1 mV (28)	-271.1 ± 0.6 mV (47)	-255.8 ± 2 mV (16)	-255.4 ± 2 mV (27)

Cardiomyocytes of mito1, mito2, cyto1 and cyto2 were isolated and incubated at 37°C and 5% CO_2 for 1 hr except for the overnight culture measurements. The measurements of the maximum oxidation and reduction response were performed upon different conditions for each mouse line. Numbers in the parentheses indicate the number of cardiomyocytes analyzed. Mean ± SEM. *$p < 0.05$ (compared to mito1 and mito2 hearts), one-way ANOVA (Bonferroni post-hoc-test).

3.6 The results of the imaging in Langendorff perfused hearts were comparable to those of the single cell measurements

The up to here described experiments were performed with isolated cells. To investigate the E_{GSH} in a more physiological context, experiments were conducted with whole hearts of all mouse lines. The mouse hearts were cut off right above the aorta and retrogradely perfused in the Langendorff mode with a Tyrode solution. During imaging, a strong signal of the ventricles was detected which demonstrates the localization of the sensor to the ventricular cardiomyocytes due to the αMHC promoter (**Figure 18**). Reaching a stable baseline, hearts were perfused subsequently with 200 µm H_2O_2, a washing step and 2 mM DTT. As observed in the isolated cardiomyocytes, the ratio of the sensor increased after the oxidative stimulation and decreased after application the reducing agent. The extent of the signal change also corresponded to the results of the isolated cells under oxidation and reduction. Both mito mouse lines revealed a higher increase upon the oxidative stimulus while the cyto mouse lines presented a higher decrease upon the reductive stimulus (**Figure 19**). This result indicates a more reduced E_{GSH} in the mitochondrial matrix as in the cytoplasm comparable to the results obtained with isolated cardiomyocytes. Calculations of OxD_{roGFP2} were also comparable to the results of isolated cardiomyocytes (**Table 9**).

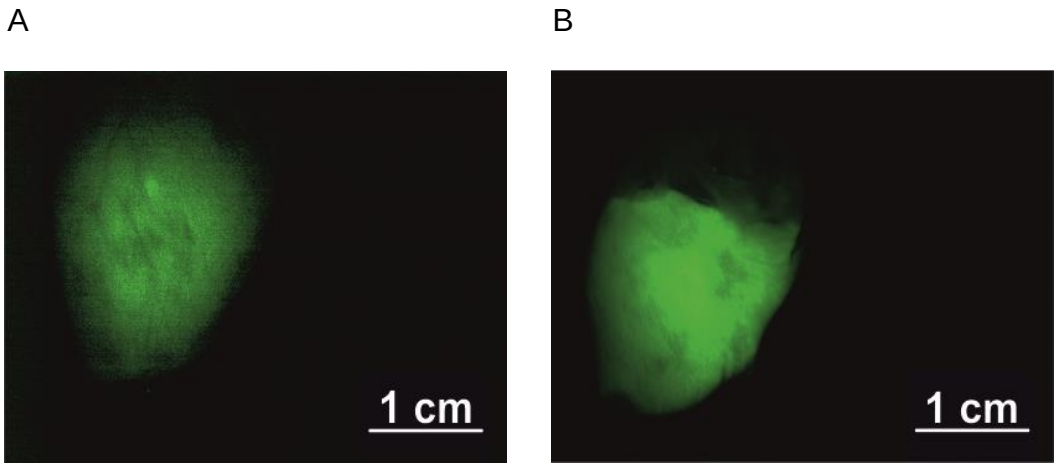

Figure 18: Both the hearts of Grx1-roGFP2 mito1 and cyto1 mice showed a clear green fluorescence signal of the ventricles. Hearts of mito1 **(A)** and cyto1 mice **(B)** were perfused with Tyrode solution via Langendorff mode and excited with 488 nm before addition of an active substance. Emission was detected at 510 nm. Both the mito1 and cyto1 heart showed a strong fluorescence signal after excitation.

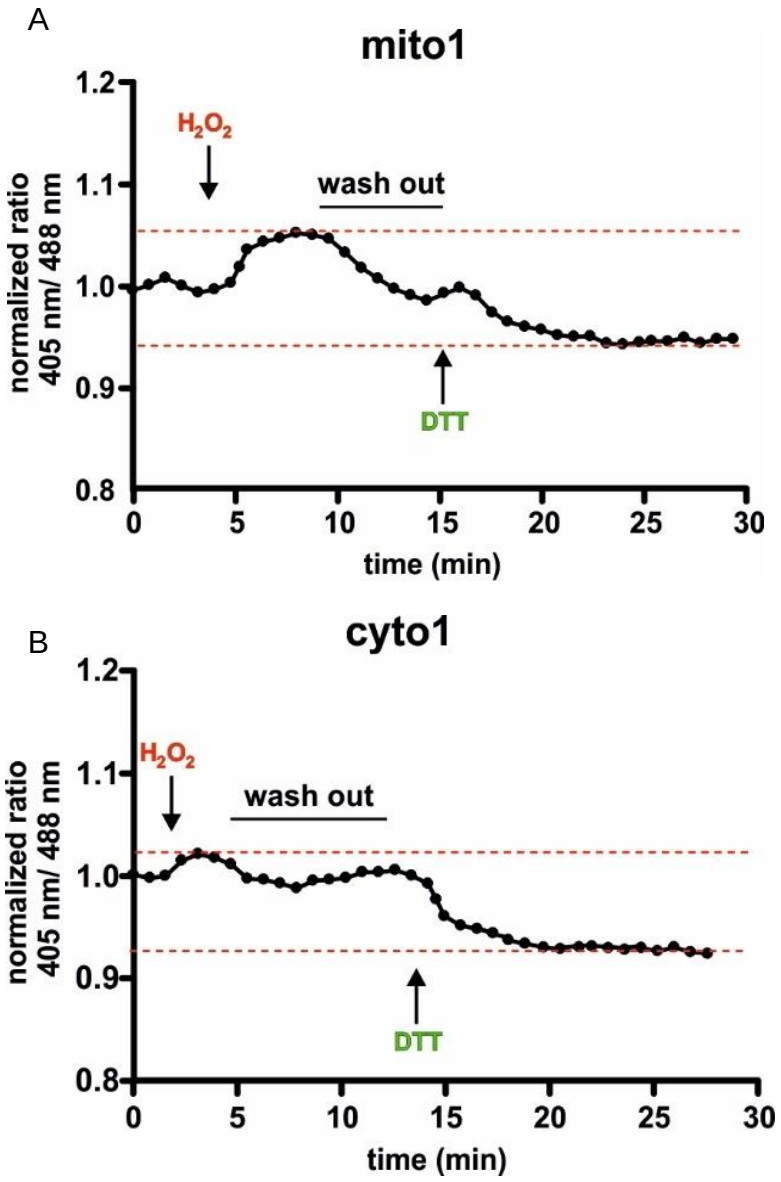

Figure 19: Whole Grx1-roGFP2 mito1 hearts react with a higher increase upon oxidation and smaller decrease upon reduction compared to Grx1-roGFP2 cyto1 hearts. Exemplary response of a mito1 **(A)** and cyto1 **(B)** hearts to a subsequent perfusion with 200 µM H_2O_2, wash out and 2 mM DTT. Ratio of the fluorescence emissions at 510 nm after excitation with 405nm and 488 nm were recorded.

Table 9: Calculation of OxD from whole heart imaging

	mito1	mito2	cyto1	cyto2
OxD H_2O_2 – DTT WHI	52.0 ± 6.1% (5)	50.0 ± 4.8% (4)	85.1 ± 7*% (5)	87.3 ± 3.9*% (9)
OxD H_2O_2 – DTT IC	52.0 ± 1.2% (104)	58.4 ± 0.7% (98)	86.8 ± 0.5*% (112)	85.5 ± 0.7*% (154)

The degree of oxidation of the Grx1-roGFP2 sensor was calculated fort both isolated cardiomyocytes and whole hearts of each mouse line. The numbers in parentheses indicate the number of animals analyzed. Mean ± SEM. *$p < 0.05$ (compared to mito1 and mito2 hearts), one-way ANOVA (Bonferroni post-hoc-test). WHI: Whole heart imaging, IC: isolated cardiomyocytes.

4 Discussion

Although reactive species have long been considered detrimental in the context of oxidative stress, ROS and RNS are nowadays known to play a central role in physiological processes controlled via redox signaling. In cardiomyocytes, redox signaling is involved starting from differentiation and proliferation through ECC and Ca^{2+} homeostasis to apoptosis (Santos et al. 2016; Burgoyne et al. 2012). In order to enable redox signaling, the redox balance is maintained by redox couples such as NADP+/NADPH, TRX-SH/TRX-SS and 2GSH/GSSG. However, an imbalance of these in favor of a strongly reducing milieu can lead to reductive stress, which is of pathophysiological importance (Narasimhan and Rajasekaran 2015; Pérez-Torres et al. 2017; Bajic et al. 2019). The redox status is no longer seen as a global cellular concept but as a characteristic of the individual redox pairs within the different subcellular compartments (Jones and Go 2010). Likewise, the development of cardiac diseases such as heart failure or myocardial I/R-injury is associated with specific subcellular sources of ROS (Hafstad et al. 2013; Cadenas 2018).

The low-weight molecular antioxidant GSH is an excellent cellular redox buffer due to its abundance and presence in a predominantly reduced form, and thus it is referred to be a useful indicator for the cellular redox status (Schafer and Buettner 2001). Changes both in concentration and the ratio of GSH:GSSG have been linked to the development and progression of CVD, and post-translational modifications such as S-glutathionylation as part of redox signaling are of particular importance (Bajic et al. 2019; Burns et al. 2020).

Conventional methods for measuring GSH and GSSG by HPLC or redox sensitive fluorescent dyes usually are not able to provide subcellular information or real time monitoring. Since redox homeostasis dynamically reflects the different redox pairs, which are neither in equilibrium with each other nor with themselves across the subcellular compartments, roGFP sensors offer an excellent opportunity to study them in both high temporal and spatial resolution (Hanschmann et al. 2013; Schwarzländer et al. 2016).

roGFP sensors have been used in several models to study E_{GSH}, but prior to our study there was no mouse model that allowed the specific analysis of E_{GSH} in the cytosol and mitochondria of cardiomyocytes. Therefore, the aim of this thesis was to analyze the developed models of Grx1-roGFP2 transgenic mice regarding their functionality and to newly investigate whether specific subcellular redox characteristics exist.

4.1 The Grx1-roGFP2 sensor is well expressed in both mitochondria and cytoplasm without altering heart function

After the generation of the Grx1-roGFP2 mouse lines cyto1, cyto2, mito1 and mito2, the percentage of roGFP2 positive cardiomyocytes was determined for each of the four mouse lines. In all four mouse lines, more than 70% of cardiomyocytes were GFP positive, with more than 90% positivity in mito1 and mito 2. In addition, the mito mouse lines had a slightly stronger signal intensity, indicating an increased abundance of the sensor compared to the cyto mouse lines. However, due to the ratiometric characteristic of roGFP2, varying sensor concentrations are not expected to affect the measurement. This has also been demonstrated by studies, which reveal a constant ratio at different signal intensities (Schwarzländer et al. 2016; Ayer et al. 2013; Bhaskar et al. 2014).

Another important aspect regarding the expression of a genetically engineered protein of about 50 kDa was to exclude that the Grx1-roGFP2 impacts cardiac function (Delorme-Hinoux et al. 2016; Kaludercic et al. 2014). Indeed, a study by Huang et al. (2000) on α-MHC gene driven transgenic eGFP mice has indicated that overexpression of eGFP, from which roGFP2 is derived, can lead to the development of cardiomyopathy, which is attributed to an increased activation of CaMKII by eGFP according to Khoo et al. (2008). Similar findings were published by Ho et al. (2007): By using a cardiac myosin light chain 2 gene, two cardiac specific zebrafish lines with different expression levels of GFP were generated. Excess expression of GFP resulted in an impairment of cardiac growth and function. In contrast, other studies with cardiac specific expression of eGFP and GFP via the hamsterβ-MHC and human α-actin promoter, respectively, in mice showed no harmful effect on cardiac performance (Xian et al. 1999; Fleischmann et al. 1998). Nevertheless, when comparing the studies, it must be kept in mind that the reduced cardiac function observed by Huang et al. (2000) and Ho et al. (2007) were not due to general expression but to overexpression of GFP. For each of our four transgenic Grx1-roGFP2 mouse lines echochardiography was performed to assess the cardiac function. As compared to wt littermates no difference of cardiac function was observed, we concluded that the expression of Grx1-roGFP2 is sufficient to allow E_{GSH} measurements but is not overexpressed to an extent that it harms the physiological function of the heart. To support the results of echocardiography, trichrome staining of Grx1-roGFP2 positive and wt mice was performed by Swain et al. (2016), whereby no morphological difference was observed. Furthermore, by comparing complex I, II, IV and V activities as well as the oxygen consumption rate of isolated mitochondria from the transgenic and wt mice, Swain et al. (2016) demonstrated that expression of Grx1-roGFP2 did not impair mitochondrial function.

4.2 The Grx1-roGFP sensor shows a dynamic and reversible response in both the cytoplasm and mitochondrial matrix

The first step to describe the steady state of E_{GSH} within the cytoplasm and mitochondria of cardiomyocytes was to calibrate the sensor to a state of maximal reduction and oxidation. Cardiac myocytes of different isolations were titrated with increasing concentrations of H_2O_2 and DTT to define the concentrations which lead to the maximal states r_{ox} and r_{red}. To confirm the reversibility of the sensor, described by Gutscher et al. (2008), single cell measurements were performed with consecutive application of H_2O_2 and DTT. However, as a higher rate of cardiomyocyte cell death occurred, we opted for single cell measurements with only H_2O_2 or DTT to determine the fully oxidized and reduced states in the further experiments, respectively. As discussed above, there were no hints for alterations of cardiac function due to the expression of the sensor. But as the cardiomyocytes were exposed to both abnormal high concentrations of H_2O_2 (at least 10-fold higher assuming an intracellular concentration of 10 nm) and the reducing agent DTT, it may lead to cell death (Sies 2017; Lyublinskaya and Antunes 2019).

To ensure that H_2O_2 reached complete sensor oxidation as it leads indirectly to the oxidation of the sensor via endogenous GSH, additional experiments were performed with diamide. These showed no significant difference in maximum oxidation compared to H_2O_2. Thus, the indirect oxidation of the sensor via H_2O_2 showed us the equilibration between oxidized GSH and our Grx1-roGFP2 sensor and the similar maxima of oxidation confirm that the endogenous GSH pool is sufficient to lead to maximal sensor oxidation.

Compared with other methods for determination of GSH in cardiomyocytes, the Grx1-roGFP2 outstands by its dynamic, reversible behavior as well as the possibility of subcellular measurements. Li et al. (2003) used mBCl to investigate cellular mechanisms affecting intracellular cardiac GSH. Isolated cardiomyocytes were treated with a solution containing mBCl, which is transferred via GST to GSH to build a fluorescent adduct. The measurement via an inverted microscope is comparable to our setting but neither subcellularly specified nor ratiometric. Limitations of mBCl are also discussed by some authors due to the accumulation of the mBCl-GSH conjugate in the nucleus and lack of specificity for GSH due to alternating activity of GST isoforms (Briviba et al. 1993; van der Ven et al. 1994). King et al. (2004) used the fluorescent dye Blue CMAC to evaluate GSH levels in freshly isolated cardiomyocytes. Similar to mBCl, Blue CMAC is transferred via GST to GSH to become a fluorescent adduct. However, Blue CMAC exhibit brighter fluorescence characteristics and its interaction with GSH was shown to be reversible (King et al. 2004). Although the calibration of measurements with Blue CMAC enabled the quantification of GSH levels upon varying conditions, there is no direct reflection of the E_{GSH} and the subcellular specification is still lacking.

Based on r_{ox} and r_{red}, the dynamic range of the Grx1-roGFP2 sensor within our model has been calculated. The dynamic range of the biosensor expressed in our mouse lines were determined to range from 4.2 to 5.0, which goes in line with other reported values of the sensor (Morgan et al. 2011; Albrecht et al. 2011). Thus, the Grx1-roGFP2 sensor provides enough sensitivity to reflect minor changes in E_{GSH} in the settings used in our study.

4.3 The cytosolic E_{GSH} is more oxidizing than the E_{GSH} of the mitochondrial matrix

Based on the maximum reduction and oxidation values, E_{GSH} for both mito and cyto mouse lines were derived according to the methods published in Meyer and Dick (2010). One of the key findings of this study is that the cytosolic E_{GSH} (-278.8 ± 0.7 mV (cyto1) and -280.3 ± 0.7 mV (cyto2)) is more oxidized than mitochondrial E_{GSH} (-333.6 ± 0.4 mV (mito1) and -330.1 ± 0.4 mV (mito2)) in cardiomyocytes.

Especially given the fact that mitochondria are often considered as the main source of ROS, these results might seem surprising. Indeed, studies on yeast postulated a more oxidizing environment in mitochondria (Monteiro et al. 2004; Outten and Culotta 2004). Rebrin et al. (2005) measured GSH:GSSG ratios in various tissues of senescence accelerated mice. Therefore, the HPLC method was used to determine both cytosolic and mitochondrial concentrations of GSH and GSSG. With respect to the cardiac tissue homogenate and isolated mitochondria a higher cytosolic GSH:GSSG ratio compared to the mitochondrial one was measured in the control group, which would indicate that the mitochondrion is more oxidized than the cytosol. According to Hu et al. (2008), the measured GSH:GSSG ratios of the studies described above would represent redox potentials of -250 mV to -280 mV at pH 7.8, which would be about 50 to 70 mV less reducing than our measurements. Measuring E_{GSH} and GSH concentrations via conventional methods like HPLC is challenging due to procedures of permeabilization and isolation and may lead to artificial oxidation of GSH (Go and Jones 2008). In line with our data are the results of studies performed by Dooley et al. (2004) and Hanson et al. (2004) on HeLa cells using the roGFP2 sensor, in which also a more reducing redox environment was found in the mitochondrion compared to the cytoplasm (cytosolic E_{GSH} -325 mV vs. matrix E_{GSH}-365 mV). Albrecht et al. (2011) used cyto-Grx1-roGFP2 and mito-roGFP2-Grx1 in *Drosophila melanogaster* to evaluate cytosolic and mitochondrial E_{GSH} in different tissues and likewise found a highly reduced mitochondrial GSH status in muscle tissue and gut enterocytes. However, this condition was not seen in other tissues such as hemocytes and fat tissue, so that the GSH redox status within the cytoplasm and mitochondrion may be characterized somewhat differently depending on tissue type and function. Overall, data obtained by fluorescent based redox probes argue for rather reducing environments in both mitochondrion and cytoplasm (Calabrese et al. 2017).

Efficient cardiac mitochondrial function is of particular importance not only due to the high aerobic metabolism of the heart but also due to their involvement in processes such as Ca^{2+} homeostasis and apoptosis (Hafstad et al. 2013; Kanaan and Harper 2017). Mitochondrial dysfunction is linked to several cardiac pathologies such as heart failure, myocardial I/R-injury and hypertrophy (Zhou and Tian 2018; Kalogeris et al. 2014; Peoples et al. 2019). Mitochondria are the most redox active compartments of the cell and yet have various defense systems to cope with reactive species (Go and Jones 2008): besides SOD, catalase and other antioxidant enzymes, GPX, using GSH as a cofactor, and Prx are the most important systems concerning detoxification of H_2O_2 (Ribas et al. 2014; Antunes et al. 2002). Furthermore, non-enzymatic and non-specific S-glutathionylation occurs at low GSH:GSSG ratios, i. e. at high levels of reactive species, causing hyperglutathionylation of proteins, which affects their activity (Ribas et al. 2014). In this regard, complex I of the MRC was shown in bovine and murine heart to be both S-glutathionylated and deglutathionylated via Grx2, whose functionality depends on the redox state of the 2GSH/GSSG couple (Mailloux and Willmore 2014; Beer et al. 2004). A persistent low (oxidized) GSH:GSSG ratio or knockout of Grx2 caused loss of complex I activity, resulting in a significant decrease in mitochondrial ATP production, which in turn was reversible upon restoration of a reducing environment (Beer et al. 2004; Mailloux et al. 2014b). A highly reducing mitochondrial E_{GSH} in cardiac myocytes, associated with a high GSH:GSSG ratio (as obtained in our experiments), thus provides a redox milieu wherein specific signaling pathways may take place and nonspecific signaling effects can be avoided. Furthermore, regeneration of GSH is highly dependent on the availability of NADPH as a reducing equivalent. Nickel et al. (2015) demonstrated, that mitochondrial Nnt, which regenerate NADPH (antioxidant cofactor) at the expense of NADH (metabolic cofactor), switches upon an increased pathological cardiac workload to a pro-oxidative mode with regeneration of NADH from NADPH, and thus contributes to increased mitochondrial ROS emission. According to this, a highly reducing mitochondrial E_{GSH} might be crucial to maintain both a balanced antioxidant defense and a sufficient metabolic function of the mitochondria, being a major source and a vulnerable target of oxidative stress in one.

Regarding the cytosolic E_{GSH}, our results indicate a more reducing cytosolic environment, in contrast to measurements via conventional methods reported in the literature: estimations of the E_{GSH} in the cytoplasm range from -260 mV to 150 mV depending on the cellular status (Jones 2002; Schafer and Buettner 2001). According to Giustarini et al. (2013) conventional measurements of GSH with disruption of the cells lead to an overestimation of the GSSG due to an artificial oxidation of the GSH, in the range of 5 - 15%. In particular, if the proportion of GSSG to GSH is low, as it is estimated to be 50:1 in conventional measurements of GSH:GSSG, this artificial oxidation could have a significant impact on the estimated E_{GSH} (Schwarzländer et al. 2016). Furthermore, estimations of cytosolic E_{GSH} were based on measurements of whole cell lysates, involving beneath the cytosol other subcellular organelles as the ER and nucleus. According to the conclusions of Schwarzländer et al.

(2016), the values obtained via conventional and GFP-based methods do not absolutely contradict each other, since there is no clear separation of the various subcellular compartments in the cell lysates, and oxidizing compartments such as the ER can have a significant influence on the measured values. Therefore, the authors also point out that the values derived from measurements with cell lysates should not be used as an estimation of cytosolic E_{GSH}.

Compared to other studies using transgenic fluorescent redox probes in non-cardiomyocytes, the cytoplasmic E_{GSH} is reported to be even more reduced than seen in our results. Throughout experiments with HeLa cells (roGFP2, -325 mV), fruit flies (Grx1-roGFP2, -300 mV), yeast (Grx1-roGFP2, -320 mV) and plants (roGFP2, -300 mV) calculated cytosolic E_{GSH} were about 20 to 40 mV more reduced (Dooley et al. 2004; Albrecht et al. 2011; Morgan et al. 2011; Meyer et al. 2007). Indeed, in our studies, the cytosolic Grx1-roGFP2 sensor is approximately 85% oxidized at steady state, whereas in other studies using a roGFP2 sensor, it is highly reduced (up to 95%) (Schwarzländer et al. 2016; Meyer et al. 2007; Xu et al. 2011). During the experiments for calibration of the sensor, a lower increase of the I405/I488 ratio was observed with the addition of H_2O_2 or diamide in the cyto mouse lines in contrast to the mito mouse lines. This indicates a higher basal OxD_{GSH} in the cytoplasm than in the mitochondrial matrix. However, since a significant increase or decrease in the ratio was seen by using both H_2O_2 and DTT, we concluded that the cytosolic E_{GSH} of the murine cardiomyocytes is within the dynamic range of the sensor. According to Meyer and Dick (2010), the sensitive range of the sensor for adequate detection lies within an OxD_{roGFP2} of 5 to 95%, and thus, the OxD_{roGFP2} of our cyto mouse lines is within these limits.

In view of these results, we had to exclude that artificial oxidation of GSH may have occurred during the process of isolation of cardiomyocytes, resulting in an influence on the subsequent measurements. Therefore, we performed additional experiments with isolated cardiomyocytes cultured overnight to exclude a potential influence of the isolation. There were no significant deviations of E_{GSH} in the cyto as well as in the mito mouse lines. During the process of isolation, we initially used a Ca^{2+} - free buffer. To prevent the phenomenon of Ca^{2+} paradox, potentially leading to extensive cellular damage and ROS production, a gradual recalcification of the isolated cardiomyocytes was performed (Chapman und Tunstall 1987; Lazou et al. 2000). To exclude the possibility of an influence of recalcification on E_{GSH}, we omitted recalcification and performed experiments with Ca^{2+}- free buffer. No significant differences compared to measurements using recalcified cardiomyocytes and Ca^{2+}-containing buffer were detected. This observation is in line with the results of Lazou et al. (2000), who found a release of both GSH and GSSG from rat cardiomyocytes after reperfusion with Ca^{2+}, whereas there was no change in the ratio of the low weight molecule and its disulfide form. In order to exclude an effect on E_{GSH} by starvation in cardiomyocytes, 10 mM glucose was added to the buffer in subsequent experiments. Similarly, no significant differences compared to measurements with glucose-free buffer were detected. Furthermore,

we analyzed whole hearts in order to determine whether the measurements on isolated cardiomyocytes differ from those in the whole heart composite. Herein, our measurements showed an OxD_{roGFP2} that is comparable to the OxD_{roGFP2} derived by single cell measurements. Therefore, it may be concluded that the process of isolation of single cardiomyocytes has no influence on the basal E_{GSH}. Beyond that, it needs to be considered that the basal cellular E_{GSH} may differ between isolated cells and cells being part of a whole organ. Trautsch et al. (2019) employed the Grx1-roGFP2 sensor via lentiviral transduction into both cardiomyocytes differentiated from human embryonic stem cells and human foreskin fibroblasts, and determined the E_{GSH} of the single cardiomyocytes and fibroblasts as well as of both cell types in engineered human myocardium. Interestingly, the E_{GSH} of the fibroblasts in the engineered myocardium (-297 mV) was more reduced than of single fibroblasts (-269mV) indicating a possible influence of the cellular milieu on the E_{GSH} (Trautsch et al. 2019). However, the E_{GSH} of the cardiomoycytes in the engineered myocardium (-284 mV) and of the single cardiomyocytes (-289 mV) exhibited comparable redox potentials. These results go in line with our findings of similar values for OxD_{roGFP2} in both single cardiomyocytes and whole hearts, which may suggest a relatively stable E_{GSH} of cardiac myocytes independent of the cellular context. Furthermore, though the values of E_{GSH} reported for cardiomyocytes by Trautsch et al. (2019) are slightly more reduced than seen in our results, they are as well more oxidized than values of E_{GSH} reported for other cell types.

When comparing our results with other reports in the literature, it is important to keep in mind that our study focuses on cardiomyocytes, which exhibit a different structure and function than keratinocytes, erythrocytes, neurons, or yeast. Cardiomyocytes are characterized by both their high aerobic metabolism and their defined contractile apparatus, all acting together as a functional syncytium. Giustarini et al. (2011) investigated the content of low molecular weight thiols, including GSH and GSSG, in various rat tissues by HPLC. On the one hand, by treating the tissue samples either with or without N-ethyl maleimide (NEM), which alkylates free SH-groups, they were able to show that artificial oxidation indeed occurs during conventional methods using tissue homogenates. On the other hand, a difference of the GSH:GSSG ratio within the different tissues was shown: the GSH:GSSG ratio measured in the cardiac tissue was remarkably lower than those measured in erythrocytes, spleen and testis. Another experiment comparing the GSH:GSSG ratio of different tissues was performed in mice by Rebrin et al. (2003). Among the different tissues of 4-month-old mice, the GSH:GSSG ratio varied from 230:1 to 36:1, the last one being measured in the heart, also indicating a more oxidizing E_{GSH} in cardiac tissue. Nevertheless, it should be noted that the values were obtained by measuring tissue homogenates via HPLC without blocking the SH-Groups with NEM and are therefore not only affected by mixing of the different subcellular compartments, but most likely also by artificial oxidation.

Taken together, there is evidence that cardiomyocytes have in contrast to other cell types a more oxidizing cytosolic E_{GSH}, which is nevertheless more reducing than the related midpoint potential of GSH at physiological concentrations (at pH 7.4 from -174 to -157 mV) (Meyer and Dick 2010; Schafer and Buettner 2001).

4.4 Limitations of the cardiomyocyte specific Grx1-roGFP2 mouse model

Using our Grx1-roGFP2 transgenic mouse model, we demonstrated that the cytoplasm and mitochondrial matrix indeed form distinct GSH redox domains within cardiomyocytes, with the matrix having a significantly more reduced E_{GSH}. Our data suggest that this is the case both in the isolated cells and in the whole organ *ex situ*. The Grx1-roGFP2 sensor provides a useful tool for *in situ* redox measurements of the heart due to its reversibility and dynamic real-time response. However, since the heart is found in a protected environment in the center of the thorax, surgical opening of the thorax would be required to make the organ optically accessible (Fujikawa et al. 2016; Breckwoldt et al. 2014). In order to measure E_{GSH} under varying conditions *in situ*, Fujikawa et al. (2016) developed a method in a mouse model to generate histological sections, which preserve the redox state and represent redox maps of different tissues. Hence, E_{GSH} can be displayed upon different conditions in organs whose optical accessibility is limited, but no dynamic measurements of E_{GSH} are possible. Dynamic measurements *in situ* in real-time are therefore reserved for very small or translucent animals (e. g. zebrafish) for the time being (Fujikawa et al. 2016; Panieri et al. 2017).

The results of our experiments using a cardiomyocyte-specific Grx1-roGFP2 sensor give us information about the E_{GSH} in the cytoplasm and mitochondrial matrix. On the one hand, E_{GSH} depends on the ratio of GSH:GSSG. However, the same ratio of GSH:GSSG would result in different E_{GSH} at different concentrations of GSH_{total}. Therefore, although our results provide important information about the E_{GSH} in the given compartments, they do not contain the entire information needed to describe the GSH homeostasis within cardiomyocytes (Oestreicher and Morgan 2019). Measurements of GSH_{total} using cell lysates range from 1 to 10 mM (Jones and Go 2010). Based on these data, the cytosolic and mitochondrial E_{GSH} derived from our experiments could be used to determine the GSH:GSSG ratio within cardiomyocytes, which varies from 3600:1 to 360:1 (cytoplasm) and 17000:1 to 1700:1 (mitochondrial matrix), respectively. In this regard, the highest potential GSH:GSSG ratio is 10-fold higher than the lowest GSH:GSSG ratio, which may have a noticeable influence on the change of the E_{GSH} under oxidizing or reducing stimuli (Schafer and Buettner 2001). A more precise method to determine GSH_{total} within subcellular compartments was developed by Montero et al. (2013). They investigated the specific ratio of GSH:GSSG in the ER using a single cysteine Grx sensor placed in the ER of HeLa cells, which attained an equilibrium between the sensor couple and the 2GSH/GSSG couple via

autocatalytic glutathionylation. Using both their results and the E_{GSH} of the ER of HeLa cells obtained by Birk et al. (2013), the GSH_{total} of the ER was calculated. Application of this method to the cytoplasm and mitochondrial matrix of cardiomyocytes, along with our results, may provide more detailed insight into subcellular cardiac GSH homeostasis.

4.5 Conclusion and outlook

On the basis of our transgenic cardiomyocyte-specific Grx1roGFP2 mouse lines, we have succeeded in performing specific studies of cytosolic and mitochondrial E_{GSH} in both isolated cells and whole hearts. In all four mouse lines analyzed, we demonstrated an appropriate expression of the Grx1-roGFP2 sensor, providing a suitable basis for redox measurements but not resulting in any impairment of cardiac function. Both reductive and oxidative stimuli resulted in an adequate, dynamic change of the fluorescence ratio, indicating that the respective E_{GSH} is within the measurement range of the Grx1-roGFP2 sensor. Titration of the sensor to reach the maximum oxidized and reduced state allowed us to determine the basal E_{GSH} for both cyto and mito mouse lines. Consistent with previously performed studies, the mitochondrial matrix showed a highly reducing E_{GSH}, whereas the cytosolic E_{GSH} is more oxidized. Compared with other studies investigating the GSH:GSSG ratio of the heart or E_{GSH} of cardiomyocytes, our results indicate that this appears to be a specific characteristic of cardiac myocytes. An E_{GSH} close to the GSH midpoint potential is more stable, since small changes in the GSH:GSSG ratio cause no large changes of E_{GSH} (Schwarzländer et al. 2016). However, given this value of cytosolic E_{GSH}, it must be taken into account that it is a general cytosolic E_{GSH}. Hatori et al. have revealed that E_{GSH} is heterogeneous within the cytosol by using different Grx1-roGFP sensors localized at the cytoskeleton or organelle membranes within the cytoplasm of HeLa cells (Hatori et al. 2018; Hatori et al. 2020). Since redox active enzymes like NOX2 and NOX4 are predominantly located at membranes and the cytosol of cardiomyocytes is characterized by the contractile apparatus, further experiments involving such specifically localized redox sensors would be desirable to investigate whether heterogeneity of cytosolic E_{GSH} is also present in cardiomyocytes. Further research is needed to assess the significance of the more oxidized cytosolic E_{GSH} in cardiomyocytes compared to other cell types. A very interesting approach is provided by Booty et al. (2019), who render mitochondrial GSH variably redox silent through the use of a mitochondrially localized 1-chloro-2,4-dinitrobenzene (MitoCDNB), which causes removal of mitochondrial GSH by formation of 1-S-glutathionyl-2,4-dinitrobenzeneemit (GSDNB). Hence, the effects of changes in mitochondrial thiol status can be examined, but along with the removal of mitochondrial GSH, the redox enzymes Trx2 and Prx3 are as well inhibited by MitoCDNB, making this approach specific to one compartment, but not exclusive to the GSH system (Booty et al. 2019; Sies and Reichert 2019). Compartment and redox pair specific, gradual changes in the GSH:GSSG ratio would

help to explore the precise influence and significance of the respective GSH pool and corresponding E_{GSH} in physiology and pathology.

The cardiomyocyte specific Grx1roGFP2 mouse models represent suitable tools to study mitochondrial and cytosolic E_{GSH} under varying conditions. Using our mouse model, Swain et al. (2016) has demonstrated that the E_{GSH} of the cytosol and the mitochondrial matrix of cardiomyocytes react and are influenced differently upon hypoxic conditions as well as under myocardial infarction, which underlines their importance as independent subcellular redox domains. Another perspective to further investigate the complexity of cellular redox homeostasis is the recent development of GFP-based sensors with different spectral properties, allowing simultaneous measurements of distinct redox couples and in the same experimental setting (Shokhina et al. 2019; Schwarzländer et al. 2016)

The analysis of cytosolic and mitochondrial E_{GSH} performed in this thesis provides a first insight into the GSH redox homeostasis in cardiomyocytes. Nevertheless, further experiments are required to gain a detailed knowledge into the physiological and pathological subcellular redox processes in order to develop therapeutic strategies to prevent and improve redox associated cardiac pathologies.

5 Abstract

In the field of redox biology, the mainly negative perception of reactive oxygen species has given way to the global concept of an intracellular redox balance. Free radicals like H_2O_2 not only lead to harmful effects within oxidative stress but are also essential for physiological processes. Redox homeostasis of cardiomyocytes is important for the maintenance of physiological function: disruption of redox balance has been linked to the development of heart failure, cardiac hypertrophy, and other cardiac pathologies. The low weight molecule glutathione, the essential cellular antioxidant, contributes to the maintenance of cellular redox homeostasis. The redox status of the glutathione is reflected by its redox potential (E_{GSH}). The development of transgenic redox sensors based on the green fluorescent protein (roGFP), which are fused to glutaredoxin-1 (Grx1), allows dynamic and specific measurements of E_{GSH} in intact cells and organs. A specific subcellular localization of the redox sensor can be achieved via targeting sequences. Thus, Grx1-roGFP2 redox sensors offer a significant advantage compared to conventional measurements, which often involve destruction of the cell or lack specificity.

The aim of this study was to characterize the cytosolic and mitochondrial E_{GSH} in cardiomyocytes using the Grx1-roGFP2 sensor. In two of the four analyzed Grx1-roGFP2 mouse lines, the redox sensor was localized to the mitochondrial matrix, whereas in the other two mouse lines the sensor was non-targeted in the cytoplasm. In all four mouse models, impairment of cardiac performance due to the sensor was excluded by echocardiography. Based on the measurement of the different fluorescence intensities of the Grx1-roGFP2 sensor depending on its oxidation state, isolated single cells in all four mouse lines were analyzed and the Grx1-roGFP2 sensor showed in each mouse line a dynamic response to oxidizing and reducing stimuli. After maximal reduction and oxidation of the Grx1-roGFP2 sensor, the E_{GSH} of the cytosol and the mitochondrial matrix was determined under consideration and exclusion of interfering factors. Here, the cytoplasm showed a significantly more oxidized E_{GSH} (-278.8 ± 0.7 mV and -280.3 ± 0.7 mV) compared to the mitochondrial matrix (-333.6 ± 0.4 mV and -330.1 ± 0.4 mV). The analysis of whole hearts *ex situ* of one non-targeted and one mouse line with the sensor targeted to the mitochondrial matrix, showed comparable results as seen in the analysis of isolated cardiomyocytes. The mitochondrial E_{GSH} is consistent with values observed in other studies using roGFP2-based sensors, while the cytosolic E_{GSH} of cardiomyocytes is in contrast more oxidized than in other cell types. The results from this thesis help to shed more light on redox homeostasis in cardiomyocytes to gain a better understanding of redox processes in cardiac physiology and pathology in the future.

6 References

Albrecht SC, Barata AG, Grosshans J, Teleman AA, Dick TP (2011): In vivo mapping of hydrogen peroxide and oxidized glutathione reveals chemical and regional specificity of redox homeostasis. Cell Metab 14, 819–829

Aller I, Rouhier N, Meyer AJ (2013): Development of roGFP2-derived redox probes for measurement of the glutathione redox potential in the cytosol of severely glutathione-deficient rml1 seedlings. Front Plant Sci 4, 506

Antunes F, Han D, Cadenas E (2002): Relative contributions of heart mitochondria glutathione peroxidase and catalase to H2O2 detoxification in in vivo conditions. Free Radic Biol Med 33, 1260–1267

Aon MA, Cortassa S, Maack C, O'Rourke B (2007): Sequential opening of mitochondrial ion channels as a function of glutathione redox thiol status. J Biol Chem 282, 21889–21900

Aquilano K, Baldelli S, Ciriolo MR (2014): Glutathione: new roles in redox signaling for an old antioxidant. Front Pharmacol 5, 196

Ayer A, Sanwald J, Pillay BA, Meyer AJ, Perrone GG, Dawes IW (2013): Distinct redox regulation in sub-cellular compartments in response to various stress conditions in Saccharomyces cerevisiae. PLoS One 8, e65240

Bajic VP, van Neste C, Obradovic M, Zafirovic S, Radak D, Bajic VB, Essack M, Isenovic ER (2019): Glutathione "Redox Homeostasis" and Its Relation to Cardiovascular Disease. Oxid Med Cell Longev 2019, 5028181

Ballatori N, Hammond CL, Cunningham JB, Krance SM, Marchan R (2005): Molecular mechanisms of reduced glutathione transport: role of the MRP/CFTR/ABCC and OATP/SLC21A families of membrane proteins. Toxicol Appl Pharmacol 204, 238–255

Ballatori N, Krance SM, Notenboom S, Shi S, Tieu K, Hammond CL (2009): Glutathione dysregulation and the etiology and progression of human diseases. Biol Chem 390, 191–214

Bedard K, Lardy B, Krause KH (2007): NOX family NADPH oxidases: not just in mammals. Biochimie 89, 1107–1112

Beer SM, Taylor ER, Brown SE, Dahm CC, Costa NJ, Runswick MJ, Murphy MP (2004): Glutaredoxin 2 catalyzes the reversible oxidation and glutathionylation of mitochondrial membrane thiol proteins: implications for mitochondrial redox regulation and antioxidant defense. J Biol Chem 279, 47939–47951

Bhaskar A, Chawla M, Mehta M, Parikh P, Chandra P, Bhave D, Kumar D, Carroll KS, Singh A (2014): Reengineering redox sensitive GFP to measure mycothiol redox potential of Mycobacterium tuberculosis during infection. PLoS Pathog 10, e1003902

Birk J, Meyer M, Aller I, Hansen HG, Odermatt A, Dick TP, Meyer AJ, Appenzeller-Herzog C (2013): Endoplasmic reticulum: reduced and oxidized glutathione revisited. J Cell Sci 126, 1604–1617

Booty LM, Gawel JM, Cvetko F, Caldwell ST, Hall AR, Mulvey JF, James AM, Hinchy EC, Prime TA, Arndt S (2019): Selective Disruption of Mitochondrial Thiol Redox State in Cells and In Vivo. Cell Chem Biol 26, 449-461.e8

Börner S, Schwede F, Schlipp A, Berisha F, Calebiro D, Lohse MJ, Nikolaev VO (2011): FRET measurements of intracellular cAMP concentrations and cAMP analog permeability in intact cells. Nat Protoc 6, 427–438

Borutaite V (2003): Inhibition of mitochondrial permeability transition prevents mitochondrial dysfunction, cytochrome c release and apoptosis induced by heart ischemia. J Mol Cell Cardiol 35, 357–366

Braun NA, Morgan B, Dick TP, Schwappach B (2010): The yeast CLC protein counteracts vesicular acidification during iron starvation. J Cell Sci 123, 2342–2350

Breckwoldt MO, Pfister FMJ, Bradley PM, Marinković P, Williams PR, Brill MS, Plomer B, Schmalz A, St Clair DK, Naumann R (2014): Multiparametric optical analysis of mitochondrial redox signals during neuronal physiology and pathology in vivo. Nat Med 20, 555–560

Brejc K, Sixma TK, Kitts PA, Kain SR, Tsien RY, Ormö M, Remington SJ (1997): Structural basis for dual excitation and photoisomerization of the Aequorea victoria green fluorescent protein. Proc Natl Acad Sci USA 94, 2306–2311

Brennan JP, Bardswell SC, Burgoyne JR, Fuller W, Schröder E, C. Kentish J, Eaton P (2006): Direct activation of Type I PKA by oxidants independently of cAMP is mediated by RI subunit interprotein disulphide bond formation. J Mol Cell Cardiol 40, 928–929

Briviba K, Fraser G, Sies H, Ketterer B (1993): Distribution of the monochlorobimane-glutathione conjugate between nucleus and cytosol in isolated hepatocytes. Biochem J 294, 631–633

Broniowska KA, Diers AR, Hogg N (2013): S-nitrosoglutathione. Biochim Biophys Acta 1830, 3173–3181

Brown GC, Borutaite V (2007): Nitric oxide and mitochondrial respiration in the heart. Cardiovasc Res 75, 283–290

Burgoyne JR, Mongue-Din H, Eaton P, Shah AM (2012): Redox signaling in cardiac physiology and pathology. Circ Res 111, 1091–1106

Burgoyne JR, Rudyk O, Cho HJ, Prysyazhna O, Hathaway N, Weeks A, Evans R, Ng T, Schröder K, Brandes RP (2015): Deficient angiogenesis in redox-dead Cys17Ser PKARIα knock-in mice. Nat Commun 6, 7920

Burns M, Rizvi SHM, Tsukahara Y, Pimentel DR, Luptak I, Hamburg NM, Matsui R, Bachschmid MM (2020): Role of Glutaredoxin-1 and Glutathionylation in Cardiovascular Diseases. Int J Mol Sci 21, 6803

Cadenas S (2018): ROS and redox signaling in myocardial ischemia-reperfusion injury and cardioprotection. Free Radic Biol Med 117, 76–89

Calabrese G, Morgan B, Riemer J (2017): Mitochondrial Glutathione: Regulation and Functions. Antioxid Redox Signal 27, 1162–1177

Cannon MB, Remington JS (2008): Redox-Sensitive Green Fluorescent Protein: Probes for Dynamic Intracellular Redox Responses. A Review. Methods Mol Biol 476, 50–64

Chalfie M, Tu Y, Euskirchen G, Ward WW, Prasher DC (1994): Green fluorescent protein as a marker for gene expression. Science 263, 802–805

Chapman RA, Tunstall J (1987): The calcium paradox of the heart. Prog Biophys Mol Biol 50, 67–96

Chattoraj M, King BA, Bublitz GU, Boxer SG (1996): Ultra-fast excited state dynamics in green fluorescent protein: multiple states and proton transfer. Proc Natl Acad Sci USA 93, 8362–8367

Chen YR, Chen CL, Pfeiffer DR, Zweier JL (2007): Mitochondrial complex II in the post-ischemic heart: oxidative injury and the role of protein S-glutathionylation. J Biol Chem 282, 32640–32654

Chen YR, Zweier JL (2014): Cardiac Mitochondria and Reactive Oxygen Species Generation. Circ Res 114, 524–537

Chen Z, Lash LH (1998): Evidence for mitochondrial uptake of glutathione by dicarboxylate and 2-oxoglutarate carriers. J Pharmacol Exp Ther 285, 608–618

Christians ES, Benjamin IJ (2012): Proteostasis and REDOX state in the heart. Am J Physiol Heart Circ Physiol 302, H24-37

Cinelli RA, Ferrari A, Pellegrini V, Tyagi M, Giacca M, Beltram F (2000): The enhanced green fluorescent protein as a tool for the analysis of protein dynamics and localization: local fluorescence study at the single-molecule level. Photochem Photobiol 71, 771–776

Couto N, Wood J, Barber J (2016): The role of glutathione reductase and related enzymes on cellular redox homoeostasis network. Free Radic Biol Med 95, 27–42

Cross CE, Halliwell B, Borish ET, Pryor WA, Ames BN, Saul RL, McCord JM, Harman D (1987): Oxygen Radicals and Human Disease. Ann Intern Med 107, 526–545

Dalle-Donne I, Rossi R, Colombo G, Giustarini D, Milzani A (2009): Protein S-glutathionylation: a regulatory device from bacteria to humans. Trends Biochem Sci 34, 85–96

Dalton TP, Chen Y, Schneider SN, Nebert DW, Shertzer HG (2004): Genetically altered mice to evaluate glutathione homeostasis in health and disease. Free Radic Biol Med 37, 1511–1526

Delorme-Hinoux V, Bangash SAK, Meyer AJ, Reichheld J-P (2016): Nuclear thiol redox systems in plants. Plant Sci 243, 84–95

Deponte M (2017): The Incomplete Glutathione Puzzle: Just Guessing at Numbers and Figures? Antioxid Redox Signal 27, 1130–1161

Dooley CT, Dore TM, Hanson GT, Jackson WC, Remington SJ, Tsien RY (2004): Imaging dynamic redox changes in mammalian cells with green fluorescent protein indicators. J Biol Chem 279, 22284–22293

Dröge W (2002): Free radicals in the physiological control of cell function. Physiol Rev 82, 47–95

Eaton P, Wright N, Hearse DJ, Shattock MJ (2002): Glyceraldehyde phosphate dehydrogenase oxidation during cardiac ischemia and reperfusion. J Mol Cell Cardiol 34, 1549–1560

Eggeling C, Widengren J, Rigler R, Seidel CA (1998): Photobleaching of Fluorescent Dyes under Conditions Used for Single-Molecule Detection: Evidence of Two-Step Photolysis. Anal Chem 70, 2651–2659

Elsliger MA, Wachter RM, Hanson GT, Kallio K, Remington SJ (1999): Structural and spectral response of green fluorescent protein variants to changes in pH. Biochemistry 38, 5296–5301

Feng Q, LU X, Jones DL, Shen J, Arnold JM (2001): Increased inducible nitric oxide synthase expression contributes to myocardial dysfunction and higher mortality after myocardial infarction in mice. Circulation 104, 700–704

Fleischmann M, Bloch W, Kolossov E, Andressen C, Müller M, Brem G, Hescheler J, Addicks K, Fleischmann B (1998): Cardiac specific expression of the green fluorescent protein during early murine embryonic development. FEBS Lett 440, 370–376

Forman HJ, Fukuto JM, Torres M (2004): Redox signaling: thiol chemistry defines which reactive oxygen and nitrogen species can act as second messengers. Am J Physiol Cell Physiol 287, C246-56

Forman HJ, Ursini F, Maiorino M (2014): An overview of mechanisms of redox signaling. J Mol Cell Cardiol 73, 2–9

Forman HJ, Zhang H, Rinna A (2009): Glutathione: overview of its protective roles, measurement, and biosynthesis. Mol Aspects Med 30, 1–12

Fridovich I (1989): Superoxide dismutases. J Biol Chem 264, 7761–7764

Fujikawa Y, Roma LP, Sobotta MC, Rose AJ, Diaz MB, Locatelli G, Breckwoldt MO, Misgeld T, Kerschensteiner M, Herzig S (2016): Mouse redox histology using genetically encoded probes. Sci Signal 9, rs1

Gallogly MM, Starke DW, Mieyal JJ (2009): Mechanistic and kinetic details of catalysis of thiol-disulfide exchange by glutaredoxins and potential mechanisms of regulation. Antioxid Redox Signal 11, 1059–1081

Giustarini D, Dalle-Donne I, Milzani A, Fanti P, Rossi R (2013): Analysis of GSH and GSSG after derivatization with N-ethylmaleimide. Nat Protoc 8, 1660–1669

Giustarini D, Dalle-Donne I, Milzani A, Rossi R (2011): Low molecular mass thiols, disulfides and protein mixed disulfides in rat tissues: influence of sample manipulation, oxidative stress and ageing. Mech Ageing Dev 132, 141–148

Go YM, Jones DP (2008): Redox compartmentalization in eukaryotic cells. Biochim Biophys Acta 1780, 1273–1290

Guarnieri C (1980): Role of oxygen in the cellular damage induced by re-oxygenation of hypoxic heart. J Mol Cell Cardiol 12, 797–808

Gutscher M, Pauleau A-L, Marty L, Brach T, Wabnitz GH, Samstag Y, Meyer AJ, Dick TP (2008): Real-time imaging of the intracellular glutathione redox potential. Nat methods 5, 553–559

Guzman JN, Sanchez-Padilla J, Wokosin D, Kondapalli J, Ilijic E, Schumacker PT, Surmeier DJ (2010): Oxidant stress evoked by pacemaking in dopaminergic neurons is attenuated by DJ-1. Nature 468, 696–700

Hafstad AD, Nabeebaccus AA, Shah AM (2013): Novel aspects of ROS signalling in heart failure. Basic Res Cardiol 108, 359

Halvey PJ, Watson WH, Hansen JM, Go YM, Samali A, Jones DP (2005): Compartmental oxidation of thiol-disulphide redox couples during epidermal growth factor signalling. J Biochem 386, 215–219

Hanschmann EM, Godoy JR, Berndt C, Hudemann C, Lillig CH (2013): Thioredoxins, glutaredoxins, and peroxiredoxins--molecular mechanisms and health significance: from cofactors to antioxidants to redox signaling. Antioxid Redox Signal 19, 1539–1605

Hanson GT, Aggeler R, Oglesbee D, Cannon M, Capaldi RA, Tsien RY, Remington SJ (2004): Investigating mitochondrial redox potential with redox-sensitive green fluorescent protein indicators. J Biol Chem 279, 13044–13053

Hare JM (2004): Nitroso-redox balance in the cardiovascular system. New Engl J Med 351, 2112–2114

Harman D (1956): Aging: A theory based on free radical and radiation chemistry. J Gerontol 11:3, 298–300

Hatori Y, Inouye S, Akagi R, Seyama T (2018): Local redox environment beneath biological membranes probed by palmitoylated-roGFP. Redox Biol 14, 679–685

Hatori Y, Kubo T, Sato Y, Inouye S, Akagi R, Seyama T (2020): Visualization of the Redox Status of Cytosolic Glutathione Using the Organelle- and Cytoskeleton-Targeted Redox Sensors. Antioxidants 9, 129

Heim R, Cubitt AB, Tsien RY (1995): Improved green fluorescence. Nature 373, 663–664

Heymes C, Bendall JK, Ratajczak P, Cave AC, Samuel JL, Hasenfuss G, Shah AM (2003): Increased myocardial NADPH oxidase activity in human heart failure. J Am Coll Cardiol 41, 2164–2171

Ho YL, Lin YH, Tsai IJ, Hsieh FJ, Tsai HJ (2007): In Vivo Assessment of Cardiac Morphology and Function in Heart-specific Green Fluorescent Zebrafish. J Formos Med Assoc 106, 181–186

Hu J, Dong L, Outten CE (2008): The redox environment in the mitochondrial intermembrane space is maintained separately from the cytosol and matrix. J Biol Chem 283, 29126–29134

Huang WY, Aramburu J, Douglas PS, Izumo S (2000): Transgenic expression of green fluorescence protein can cause dilated cardiomyopathy. Nat Med 6, 482–483

Hurd TR, Requejo R, Filipovska A, Brown S, Prime TA, Robinson AJ, Fearnley IM, Murphy MP (2008): Complex I within oxidatively stressed bovine heart mitochondria is glutathionylated on Cys-531 and Cys-704 of the 75-kDa subunit: potential role of CYS residues in decreasing oxidative damage. J Biol Chem 283, 24801–24815

Infante T, Costa D, Napoli C (2021): Novel Insights Regarding Nitric Oxide and Cardiovascular Diseases. Angiology 72, 411–425

Jaimes EA, DeMaster EG, Tian RX, Raij L (2004): Stable compounds of cigarette smoke induce endothelial superoxide anion production via NADPH oxidase activation. Arterioscler Thromb Vasc Biol 24, 1031–1036

Jain M, Brenner DA, Cui L, Lim CC, Wang B, Pimentel DR, Koh S, Sawyer DB, Leopold JA, Handy DE (2003): Glucose-6-phosphate dehydrogenase modulates cytosolic redox status and contractile phenotype in adult cardiomyocytes. Circ Res 93, e9-16

Jones DP (2002): Redox potential of GSH/GSSG couple: Assay and biological significance. Meth Enzymol 348, 93–112

Jones DP (2006): Redefining Oxidative Stress. Antioxid Redox Signal 8:9-10, 1865–1879

Jones DP, Go YM (2010): Redox compartmentalization and cellular stress. Diabetes Obes Metab 12, 116–125

Kalogeris T, Bao Y, Korthuis RJ (2014): Mitochondrial reactive oxygen species: a double edged sword in ischemia/reperfusion vs preconditioning. Redox Biol 2, 702–714

Kaludercic N, Deshwal S, Di Lisa F (2014): Reactive oxygen species and redox compartmentalization. Front Physiol 5, 285

Kaludercic N, Takimoto E, Nagayama T, Feng N, Lai EW, Bedja D, Chen K, Gabrielson KL, Blakely RD, Shih JC (2010): Monoamine oxidase A-mediated enhanced catabolism of norepinephrine contributes to adverse remodeling and pump failure in hearts with pressure overload. Circ Res 106, 193–202

Kanaan GN, Harper ME (2017): Cellular redox dysfunction in the development of cardiovascular diseases. Biochim Biophys Acta Gen Subj 1861, 2822–2829

Khoo MSC, Grueter CE, Eren M, Yang J, Zhang R, Bass MA, Lwin ST, Mendes LA, Vaughan DE, Colbran RJ (2008): Calmodulin kinase II inhibition disrupts cardiomyopathic effects of enhanced green fluorescent protein. J Mol Cell Cardiol 44, 405–410

King N, Korolchuk S, McGivan JD, Suleiman MS (2004): A new method of quantifying glutathione levels in freshly isolated single superfused rat cardiomyocytes. J Pharmacol Toxicol Methods 50, 215–222

Kinugasa Y, Ogino K, Furuse Y, Shiomi T, Tsutsui H, Yamamoto T, Igawa O, Hisatome I, Shigemasa C (2003): Allopurinol improves cardiac dysfunction after ischemia-reperfusion via reduction of oxidative stress in isolated perfused rat hearts. Circ J 67, 781–787

Kirlin WG, Cai J, Thompson SA, Diaz D, Kavanagh TJ, Jones DP (1999): Glutathione redox potential in response to differentiation and enzyme inducers. Free Radic Biol Med 27, 1208–1218

Klatt P, Lamas S (2000): Regulation of protein function by S-glutathiolation in response to oxidative and nitrosative stress. Eur J Biochem 267, 4928–4944

Klomsiri C, Karplus PA, Poole LB (2011): Cysteine-based redox switches in enzymes. Antioxid Redox Signal 14, 1065–1077

Kostyuk AI, Panova AS, Kokova AD, Kotova DA, Maltsev DI, Podgorny OV, Belousov VV, Bilan DS (2020): In Vivo Imaging with Genetically Encoded Redox Biosensors. Int J Mol Sci 21, 8164

Kuroda J, Ago T, Matsushima S, Zhai P, Schneider MD, Sadoshima J (2010): NADPH oxidase 4 (Nox4) is a major source of oxidative stress in the failing heart. Proc Natl Acad Sci USA 107, 15565–15570

Lacza Z, Pankotai E, Busija DW (2009): Mitochondrial nitric oxide synthase: current concepts and controversies. Front Biosci 14, 4436–4443

Lakshmi SVV, Padmaja G, Kuppusamy P, Kutala VK (2009): Oxidative stress in cardiovascular disease. Indian J Biochem Biophys 46, 421–440

Lazou A, Seraskeris S, Tsiona V, Drossos G (2000): Oxidative status and anti-oxidant enzyme activity during calcium paradox in the rat isolated heart. Clin Exp Pharmacol Physiol 27, 160–166

Lee JD, Cai Q, Shu XO, Nechuta SJ (2017): The Role of Biomarkers of Oxidative Stress in Breast Cancer Risk and Prognosis: A Systematic Review of the Epidemiologic Literature. J Womens Health (Larchmt) 26, 467–482

Li S, Li X, Rozanski GJ (2003): Regulation of glutathione in cardiac myocytes. J Mol Cell Cardiol 35, 1145–1152

Lillig CH, Berndt C, Holmgren A (2008): Glutaredoxin systems. Biochim Biophys Acta 1780, 1304–1317

Lipinski B (2011): Hydroxyl radical and its scavengers in health and disease. Oxid Med Cell Longev 2011, 809696

Llopis J, McCaffery JM, Miyawaki A, Farquhar MG, Tsien RY (1998): Measurement of cytosolic, mitochondrial, and Golgi pH in single living cells with green fluorescent proteins. Proc Natl Acad Sci USA 95, 6803–6808

Lo Conte M, Carroll KS: The Chemistry of Thiol Oxidation and Detection. In: Jakob, U., Reichmann, D. (eds.). Oxidative Stress and Redox Regulation: Springer Netherlands. Dordrecht 2013, 1–42

Looi YH, Grieve DJ, Siva A, Walker SJ, Anilkumar N, Cave AC, Marber M, Monaghan MJ, Shah AM (2008): Involvement of Nox2 NADPH oxidase in adverse cardiac remodeling after myocardial infarction. Hypertension 51, 319–325

Lu SC (2009): Regulation of glutathione synthesis. Mol Aspects Med 30, 42–59

Lu SC (2013): Glutathione synthesis. Biochim Biophys Acta 1830, 3143–3153

Lyublinskaya O, Antunes F (2019): Measuring intracellular concentration of hydrogen peroxide with the use of genetically encoded H2O2 biosensor HyPer. Redox Biol 24, 101200

Mailloux RJ, Jin X, Willmore WG (2014a): Redox regulation of mitochondrial function with emphasis on cysteine oxidation reactions. Redox Biol 2, 123–139

Mailloux RJ, Willmore WG (2014): S-glutathionylation reactions in mitochondrial function and disease. Front Cell Dev Biol 2, 68

Mailloux RJ, Xuan JY, McBride S, Maharsy W, Thorn S, Holterman CE, Kennedy CRJ, Rippstein P, deKemp R, Da Silva J (2014b): Glutaredoxin-2 is required to control oxidative phosphorylation in cardiac muscle by mediating deglutathionylation reactions. J Biol Chem 289, 14812–14828

Maritim AC, Sanders RA, Watkins JB (2003): Diabetes, oxidative stress, and antioxidants: A review. J Biochem Mol Toxicol 17, 24–38

Matsui R, Ferran B, Oh A, Croteau D, Di Shao, Han J, Pimentel DR, Bachschmid MM (2020): Redox Regulation via Glutaredoxin-1 and Protein S-Glutathionylation. Antioxid Redox Signal 32, 677–700

Meech SR (2009): Excited state reactions in fluorescent proteins. Chem Soc Rev 38, 2922–2934

Meister A (1988): Glutathione metabolism and its selective modification. J Biol Chem 263, 17205–17208

Meister A, Anderson ME (1983): Glutathione. Annu Rev Biochem 52, 711–760

Meng Q, Peng Z, Chen L, Si J, Dong Z, Xia Y (2010): Nuclear Factor-κB modulates cellular glutathione and prevents oxidative stress in cancer cells. Cancer Lett 299, 45–53

Meyer AJ, Brach T, Marty L, Kreye S, Rouhier N, Jacquot JP, Hell R (2007): Redox-sensitive GFP in Arabidopsis thaliana is a quantitative biosensor for the redox potential of the cellular glutathione redox buffer. Plant J 52, 973–986

Meyer AJ, Dick TP (2010): Fluorescent protein-based redox probes. Antioxid Redox Signal 13, 621–650

Michiels C (2004): Physiological and Pathological Responses to Hypoxia. Am J Pathol 164, 1875–1882

Mieyal JJ, Gallogly MM, Qanungo S, Sabens EA, Shelton MD (2008): Molecular mechanisms and clinical implications of reversible protein S-glutathionylation. Antioxid Redox Signal 10, 1941–1988

Minhas KM, Saraiva RM, Schuleri KH, Lehrke S, Zheng M, Saliaris AP, Berry CE, Barouch LA, Vandegaer KM, Li D (2006): Xanthine oxidoreductase inhibition causes reverse remodeling in rats with dilated cardiomyopathy. Circ Res 98, 271–279

Monteiro G, Kowaltowski AJ, Barros MH, Netto LES (2004): Glutathione and thioredoxin peroxidases mediate susceptibility of yeast mitochondria to Ca(2+)-induced damage. Arch Biochem Biophys 425, 14–24

Montero D, Tachibana C, Rahr Winther J, Appenzeller-Herzog C (2013): Intracellular glutathione pools are heterogeneously concentrated. Redox Biol 1, 508–513

Morawietz H (2018): Cardiovascular protection by Nox4. Cardiovasc Res 114, 353–355

Morgan B, Sobotta MC, Dick TP (2011): Measuring E(GSH) and H2O2 with roGFP2-based redox probes. Free Radic Biol Med 51, 1943–1951

Muller F (2000): The nature and mechanism of superoxide production by the electron transport chain: Its relevance to aging. J Am Aging Assoc 23, 227–253

Musaogullari A, Chai YC (2020): Redox Regulation by Protein S-Glutathionylation: From Molecular Mechanisms to Implications in Health and Disease. Int J Mol Sci 21, 8113

Nakagami H (2003): NADPH oxidase-derived superoxide anion mediates angiotensin II-induced cardiac hypertrophy. J Mol Cell Cardiol 35, 851–859

Narasimhan M, Rajasekaran NS (2015): Reductive potential - a savior turns stressor in protein aggregation cardiomyopathy. Biochim Biophys Acta 1852, 53–60

Nickel AG, von Hardenberg A, Hohl M, Löffler JR, Kohlhaas M, Becker J, Reil JC, Kazakov A, Bonnekoh J, Stadelmaier M (2015): Reversal of Mitochondrial Transhydrogenase Causes Oxidative Stress in Heart Failure. Cell Metab 22, 472–484

Oestreicher J, Morgan B (2019): Glutathione: subcellular distribution and membrane transport 1. Biochem Cell Biol 97, 270–289

Ormö M, Cubitt AB, Kallio K, Gross LA, Tsien RY, Remington SJ (1996): Crystal structure of the Aequorea victoria green fluorescent protein. Science 273, 1392–1395

Østergaard H, Tachibana C, Winther JR (2004): Monitoring disulfide bond formation in the eukaryotic cytosol. J Cell Biol 166, 337–345

Outten CE, Culotta VC (2004): Alternative start sites in the Saccharomyces cerevisiae GLR1 gene are responsible for mitochondrial and cytosolic isoforms of glutathione reductase. J Biol Chem 279, 7785–7791

Pacher P, Beckman JS, Liaudet L (2007): Nitric oxide and peroxynitrite in health and disease. Physiol Rev 87, 315–424

Panieri E, Millia C, Santoro MM (2017): Real-time quantification of subcellular H2O2 and glutathione redox potential in living cardiovascular tissues. Free Radic Biol Med 109, 189–200

Pastore A, Federici G, Bertini E, Piemonte F (2003): Analysis of glutathione: implication in redox and detoxification. Clin Chim Acta 333, 19–39

Peoples JN, Saraf A, Ghazal N, Pham TT, Kwong JQ (2019): Mitochondrial dysfunction and oxidative stress in heart disease. Exp Mol Med 51, 1–13

Pérez-Torres I, Guarner-Lans V, Rubio-Ruiz ME (2017): Reductive Stress in Inflammation-Associated Diseases and the Pro-Oxidant Effect of Antioxidant Agents. Int J Mol Sci 18, 2098

Perrelli MG, Pagliaro P, Penna C (2011): Ischemia/reperfusion injury and cardioprotective mechanisms: Role of mitochondria and reactive oxygen species. World J Cardiol 3, 186–200

Poderoso JJ, Helfenberger K, Poderoso C (2019): The effect of nitric oxide on mitochondrial respiration. Nitric Oxide 88, 61–72

Poole LB (2015): The basics of thiols and cysteines in redox biology and chemistry. Free Radic Biol Med 80, 148–157

Prosser BL, Ward CW, Lederer WJ (2011): X-ROS signaling: rapid mechano-chemo transduction in heart. Science 333, 1440–1445

Rahman I, Smith CA, Antonicelli F, MacNee W (1998): Characterisation of gamma-glutamylcysteine synthetase-heavy subunit promoter: a critical role for AP-1. FEBS Lett 427, 129–133

Rahman T, Hosen I, Islam MMT, Shekhar HU (2012): Oxidative stress and human health. Adv Biosci Biotechnol 03, 997–1019

Ralser M, Wamelink MM, Kowald A, Gerisch B, Heeren G, Struys EA, Klipp E, Jakobs C, Breitenbach M, Lehrach H (2007): Dynamic rerouting of the carbohydrate flux is key to counteracting oxidative stress. J Biol 6, 10

Rebrin I, Kamzalov S, Sohal RS (2003): Effects of Age and Caloric Restriction on Glutathione Redox State in Mice. Free Radic Biol Med 35, 626–635

Rebrin I, Zicker S, Wedekind KJ, Paetau-Robinson I, Packer L, Sohal RS (2005): Effect of antioxidant-enriched diets on glutathione redox status in tissue homogenates and mitochondria of the senescence-accelerated mouse. Free Radic Biol Med 39, 549–557

Ribas V, García-Ruiz C, Fernández-Checa JC (2014): Glutathione and mitochondria. Front Pharmacol 5, 151

Richman PG, Meister A (1975): Regulation of gamma-glutamyl-cysteine synthetase by nonallosteric feedback inhibition by glutathione. J Biol Chem 250, 1422–1426

Sag CM, Wagner S, Maier LS (2013): Role of oxidants on calcium and sodium movement in healthy and diseased cardiac myocytes. Free Radic Biol Med 63, 338–349

Santos CX, Anilkumar N, Zhang M, Brewer AC, Shah AM (2011): Redox signaling in cardiac myocytes. Free Radic Biol Med 50, 777–793

Santos CXC, Raza S, Shah AM (2016): Redox signaling in the cardiomyocyte: From physiology to failure. Int J Biochem Cell Biol 74, 145–151

Schafer FQ, Buettner GR (2001): Redox environment of the cell as viewed through the redox state of the glutathione disulfide/glutathione couple. Free Radic Biol Med 30, 1191–1212

Schwarzländer M, Dick TP, Meyer AJ, Morgan B (2016): Dissecting Redox Biology Using Fluorescent Protein Sensors. Antioxid Redox Signal 24, 680–712

Schwarzländer M, Fricker M, Müller C, Marty L, Brach T, Novak J, Sweetlove L, Hell R, Meyer A (2008): Confocal imaging of glutathione redox potential in living plant cells. J Microsc 231, 299–316

Sharma P, Raghavan SAV, Saini R, Dikshit M (2004): Ascorbate-mediated enhancement of reactive oxygen species generation from polymorphonuclear leukocytes: modulatory effect of nitric oxide. J Leukoc Biol 75, 1070–1078

Shimomura O, Johnson FH, Saiga Y (1962): Extraction, purification and properties of aequorin, a bioluminescent protein from the luminous hydromedusan, Aequorea. J Cell Comp Physiol 59, 223–239

Shokhina AG, Kostyuk AI, Ermakova YG, Panova AS, Staroverov DB, Egorov ES, Baranov MS, van Belle GJ, Katschinski DM, Belousov VV (2019): Red fluorescent redox-sensitive biosensor Grx1-roCherry. Redox Biol 21, 101071

Sies H (2015): Oxidative stress: A concept in redox biology and medicine. Redox Biol 4, 180–183

Sies H (2017): Hydrogen peroxide as a central redox signaling molecule in physiological oxidative stress: Oxidative eustress. Redox Biol 11, 613–619

Sies H, Reichert AS (2019): Selectively Addressing Mitochondrial Glutathione and Thioredoxin Redox Systems. Cell Chem Biol 26, 316–318

Sies H, Sharov VS, Klotz LO, Briviba K (1997): Glutathione peroxidase protects against peroxynitrite-mediated oxidations. A new function for selenoproteins as peroxynitrite reductase. J Biol Chem 272, 27812–27817

Silter M, Kögler H, Zieseniss A, Wilting J, Schäfer K, Toischer K, Rokita AG, Breves G, Maier LS, Katschinski DM (2010): Impaired Ca(2+)-handling in HIF-1alpha(+/-) mice as a consequence of pressure overload. Pflugers Arch 459, 569–577

Slater AF, Stefan C, Nobel I, van den Dobbelsteen DJ, Orrenius s (1995): Signalling mechanisms and oxidative stress in apoptosis. Toxicol Lett 82-83, 149–153

Smyrnias I, Zhang X, Zhang M, Murray TVA, Brandes RP, Schröder K, Brewer AC, Shah AM (2015): Nicotinamide adenine dinucleotide phosphate oxidase-4-dependent upregulation of nuclear factor erythroid-derived 2-like 2 protects the heart during chronic pressure overload. Hypertension 65, 547–553

Swain L, Kesemeyer A, Meyer-Roxlau S, Vettel C, Zieseniss A, Güntsch A, Jatho A, Becker A, Nanadikar MS, Morgan B (2016): Redox Imaging Using Cardiac Myocyte-Specific Transgenic Biosensor Mice. Circ Res 119, 1004–1016

Tauskela JS, Hewitt K, Kang L-P, Comas T, Gendron T, Hakim A, Hogan M, Durkin J, Morley P (2000): Evaluation of glutathione-sensitive fluorescent dyes in cortical culture. Glia 30, 329–341

Trautsch I, Heta E, Soong PL, Levent E, Nikolaev VO, Bogeski I, Katschinski DM, Mayr M, Zimmermann W-H (2019): Optogenetic Monitoring of the Glutathione Redox State in Engineered Human Myocardium. Front Physiol 10, 272

Tsien RY (1998): The green fluorescent protein. Annu Rev Biochem 67, 509–544

Underbakke ES, Iavarone AT, Chalmers MJ, Pascal BD, Novick S, Griffin PR, Marletta MA (2014): Nitric oxide-induced conformational changes in soluble guanylate cyclase. Structure 22, 602–611

van der Ven AJ, Mier P, Peters WH, Dolstra H, van Erp PE, Koopmans PP, van der Meer JW (1994): Monochlorobimane does not selectively label glutathione in peripheral blood mononuclear cells. Anal Biochem 217, 41–47

Wang H, Viatchenko-Karpinski S, Sun J, Györke I, Benkusky NA, Kohr MJ, Valdivia HH, Murphy E, Györke S, Ziolo MT (2010): Regulation of myocyte contraction via neuronal nitric oxide synthase: role of ryanodine receptor S-nitrosylation. J Physiol 588, 2905–2917

Wang SB, Murray CI, Chung HS, van Eyk JE (2013): Redox regulation of mitochondrial ATP synthase. Trends Cardiovasc Med 23, 14–18

Wild AC, Moinova HR, Mulcahy RT (1999): Regulation of gamma-glutamylcysteine synthetase subunit gene expression by the transcription factor Nrf2. J Biol Chem 274, 33627–33636

Wilkins HM, Kirchhof D, Manning E, Joseph JW, Linseman DA (2013): Mitochondrial glutathione transport is a key determinant of neuronal susceptibility to oxidative and nitrosative stress. J Biol Chem 288, 5091–5101

Winkler BS, Orselli SM, Rex TS (1994): The redox couple between glutathione and ascorbic acid: A chemical and physiological perspective. Free Radic Biol Med 17, 333–349

Winterbourn CC, Hampton MB (2008): Thiol chemistry and specificity in redox signaling. Free Radic Biol Med 45, 549–561

Wolf AM, Nishimaki K, Kamimura N, Ohta S (2014): Real-time monitoring of oxidative stress in live mouse skin. J Invest Dermatol 134, 1701–1709

Xian M, Honbo N, Zhang J, Liew CC, Karliner JS, Lau YF (1999): The green fluorescent protein is an efficient biological marker for cardiac myocytes. J Mol Cell Cardiol 31, 2155–2165

Xu X, Löhneysen K von, Soldau K, Noack D, Vu A, Friedman JS (2011): A novel approach for in vivo measurement of mouse red cell redox status. Blood 118, 3694–3697

Yang F, Moss LG, Phillips GN (1996a): The molecular structure of green fluorescent protein. Nature Biotechnology 14, 1246–1251

Yang TT, Cheng L, Kain SR (1996b): Optimized codon usage and chromophore mutations provide enhanced sensitivity with the green fluorescent protein. Nucleic Acids Res 24, 4592–4593

Zhang GX, Lu XM, Kimura S, Nishiyama A (2007): Role of mitochondria in angiotensin II-induced reactive oxygen species and mitogen-activated protein kinase activation. Cardiovasc Res 76, 204–212

Zhang H, Forman HJ (2012): Glutathione synthesis and its role in redox signaling. Semin Cell Dev Biol 23, 722–728

Zhang M, Brewer AC, Schröder K, Santos CXC, Grieve DJ, Wang M, Anilkumar N, Yu B, Dong X, Walker SJ (2010): NADPH oxidase-4 mediates protection against chronic load-induced stress in mouse hearts by enhancing angiogenesis. Proc Natl Acad Sci USA 107, 18121–18126

Zhou B, Tian R (2018): Mitochondrial dysfunction in pathophysiology of heart failure. J Clin Invest 128, 3716–3726

Zhou T, Chuang CC, Zuo L (2015): Molecular Characterization of Reactive Oxygen Species in Myocardial Ischemia-Reperfusion Injury. Biomed Res Int 2015, 864946

Danksagung

Auf diesem Wege möchte ich mich bei allen Beteiligten bedanken, die auf unterschiedlichsten Wegen zum Gelingen dieser Arbeit beigetragen haben. Dabei möchte ich insbesondere den nachfolgenden Personen meinen Dank aussprechen.

Hauptsächlich danken möchte ich meiner Doktormutter Frau Prof. Dr. Dörthe M. Katschinski, dass ich als Teil ihrer Arbeitsgruppe an diesem aufregenden Projekt mitwirken durfte und einen spannenden Einblick in die wissenschaftliche Arbeit erhalten habe. Überaus dankbar bin ich für die hervorragende Betreuung während des Forschungsprojekts sowie die konstante Unterstützung während der Fertigstellung dieser Dissertation.

Mein herzlicher Dank gilt auch meiner Betreuerin Frau Dr. Liza Swain, welche mich in die Arbeit im Labor eingeführt und mir jederzeit mit ihrem großen Wissen und Ratschlägen zur Seite gestanden hat. Vielen Dank für die geduldige Hilfe und exzellente Zusammenarbeit während des gesamten Projekts.

Weiterhin möchte ich Frau Annette Hillemann für die großartige Zusammenarbeit und technische Unterstützung sowie die stete Hilfsbereitschaft während des Forschungsprojekts als auch danach meinen Dank aussprechen.

Darüber hinaus bedanke ich mich nachdrücklich bei Herrn Prof. Dr. Viacheslav O. Nikolaev für die Unterstützung während des Projekts. Die Bereitstellung seines Labors sowie die methodische Hilfestellung durch ihn und seine Arbeitsgruppe an der UMG bei der Isolation der Kardiomyozyten und der Fluoreszenz-Bildgebung hat einen bedeutenden Teil zu dieser Arbeit beigetragen.

Ebenso danke ich Frau Dr. Aline Jatho für die Durchführung und Auswertung der Echokardiographien sowie ihr und den anderen Mitarbeiterinnen und Mitarbeitern des Instituts für Herz- und Kreislaufphysiologie für die anhaltende Hilfsbereitschaft und produktive Arbeitsatmosphäre.

Herzlichen Dank an alle Beteiligten des Internationalen Graduiertenkollegs 1816 für die unterstützende Gemeinschaft und anregende Atmosphäre, welche durch spannende Vorträge und großartige Veranstaltungen geprägt sind. Es hat mich sehr gefreut, ein Teil davon zu sein.